DESIGN, DEVELOPMENT AND FLIGHT TESTING OF A TUBE-LAUNCHED, ROTARY-WING, MICRO AIR VEHICLE

A Thesis

by

HUNTER J. DENTON

Submitted to the Office of Graduate and Professional Studies of
Texas A&M University
in partial fulfillment of the requirements for the degree of

MASTER OF SCIENCE

Chair of Committee,	Moble Benedict
Committee Members,	Edward White
	Sivakumar Rathinam
Head of Department,	Srinivas Vadali

May 2021

Major Subject: Aerospace Engineering

Copyright 2021 Hunter J. Denton

ABSTRACT

This thesis describes the development and flight testing of a compact, re-configurable, rotary-wing micro air vehicle concept capable of sustained hover and could potentially be launched from a 40mm grenade launcher when scaled down. By launching these energy-constrained platforms to a target area, the mission range could be significantly improved. The vehicle design features coaxial rotors with foldable blades, and a thrust-vectoring mechanism for pitch and roll control. Yaw control was accomplished with a specialized counter-rotating motor system composed of two independently controlled motors. Passive unfolding of the coaxial rotor blades in flight utilizing centrifugal force was demonstrated. A cascaded feedback control strategy was implemented on a 1.7 gram custom-designed autopilot. Systematic wind tunnel tests were conducted with the vehicle on a single degree-of-freedom stand, which proved the ability of the controller to reject wind gusts up to 6 m/s and stabilize the vehicle during the powered axial descent phase. Free flight testing verified that the vehicle could hover and fly forward in winds up to 5 m/s. In-flight drop tests were conducted by throttling down the vehicle from a high altitude to attain high decent speeds followed by recovery using the rotor thrust to aggressively brake the descent and achieve a stable hover. Finally, the 366 gram vehicle was launched vertically from a pneumatic cannon followed by a stable projectile phase utilizing the fins, passive rotor unfolding, and final transition to a stable hover from arbitrarily large attitude angles demonstrating the robustness of the controller.

DEDICATION

To my parent, grandparents, and sister who have always supported and encouraged me.

ACKNOWLEDGMENTS

I would like to begin by thanking my advisor and committee chair, Dr. Moble Benedict. I met Dr. Benedict when I was a sophomore seeking a research opportunity, and under his guidance, I have gained invaluable research experience. From my undergraduate project to the GoFly Prize, Dr. Benedict pushed me to challenge myself and become a better engineer. I cannot thank him enough for giving me an opportunity to work under him and learn from his experience. I want to thank the rest my committee members, Dr. White and Dr. Rathinam, for agreeing to serve on my committee.

I would also like to thank my ARL supervisor, Dr Hao Kang who enable me to take part in an exciting research opportunity. From the first day, I learned about the tube-launch MAV project, I was eager to embrace this interesting challenge. Dr. Kang was also instrumental in helping me securing an internship at the Army Research Lab and applying for the Journeyman Fellowship.

To my fellow coworkers and friends in the Advanced Vertical Flight Lab, I would like to thank you all for making my time in the basement of Bright more bearable. Whether it was consulting about different issues with my research project or putting up with my bad jokes. I would especially like to thank Carl Runco and David Coleman for helping me when I first started working in the lab. I would also like to thank Faird Saemi for putting up with me as a roommate and keeping me sane throughout graduate school. Honestly, we have both kept each over sane over the past few years.

Finally, I want to thank my parents and sister for always being there to support me throughout my time in graduate school. I would not have made it this far without their constant love and encouragement. Additional, I would like to thank my many aunts and uncles as well as my grandparents for checking up on me from time to time.

CONTRIBUTORS AND FUNDING SOURCES

Contributors

This work was supervised by a thesis committee consisting of Professor Moble Benedict (advisor), Professor Edward White of the Department of Aerospace Engineering, and Professor Sivakumar Rathinam of the Department of Mechanical Engineering.

The flight controller used for this research was developed by Dr. Vikram Hrishikeshavan from the department of Aerospace Engineering at the University of Maryland, and the flight controls code was modified with the assistance of Dr. Hrishikeshavan and David Coleman. Undergraduate research assistants, Grant Erickson and Grant McCurdy, provided assistance during wind tunnel and flight testing presented in Chapters 7 and 8. All other work for the thesis was completed independently by the student.

Funding Sources

This work is supported by the Army Research Laboratory (ARL) and was accomplished under Cooperative Agreement Number W911NF-19-2-0057. The views and conclusions contained in this document are those of the authors and should not be interpreted as representing the official policies, either expressed or implied, of the Army Research Laboratory or the U.S. Government. The U.S. Government is authorized to reproduce and distribute reprints for Government purposes notwithstanding any copyright notation herein.

Graduate study was supported by the Journeyman Fellowship from Oak Ridge Associated Universities (ORAU).

NOMENCLATURE

A	Rotor disk area, πR^2, m^2
AC	Aerodynamic center
CG	Center of gravity
COTS	Commercial-off-the-shelf
C_Q	Coefficient of torque, $Q/\rho A\Omega^2 R^3$
C_T	Coefficient of thrust, $T/\rho A(\Omega R)^2$
DARPA	Defense Advanced Research Projects Agency
DL	Disk loading, T/A, N/m^2
FM	Figure of merit, $C_T^{3/2}/\sqrt{2}C_Q$
GTOW	Gross take off weight, N
MAV	Micro air vehicle
p	Roll body rate, deg/s
ϕ	Roll Euler angle, deg
q	Pitch body rate, deg/s
Q_1	Upper rotor aerodynamic torque, Nm
Q_2	Lower rotor aerodynamic torque, Nm
r	Yaw body rate, deg/s
ρ	Air density, kg/m^2
R	Rotor radius, m
rpm	Rounds per minute
θ	Pitch Euler angle, deg
T	Rotor thrust, N

UAV	Unmanned Aerial vehicle
V_∞	Freestream velocity, m/s
Ω	Rotation speed of rotor, rad/s

TABLE OF CONTENTS

Page

LIST OF FIGURES

FIGURE Page

LIST OF TABLES

TABLE Page

1. INTRODUCTION AND LITERATURE REVIEW

1.1 Background and Motivation

1.1.1 Micro Air Vehicles

In recent years, unmanned aerial vehicles (UAVs) have became widely popular for military and commercial applications. UAVs are a category of flying vehicles, which includes fixed-wing, flapping-wing, rotary-wing, as well as other exotic forms of propulsion, that are controlled remotely or autonomously without the need of a human pilot onboard and can carry useful payloads such as sensors or cameras. These vehicles have been developed over a range of scales from palm-sized at the smaller end to Group-4 UAVs, which are comparable to their manned counterparts. Many of these vehicles are used in activities such as land surveying, aerial photography, reconnaissance, and many other applications.

Over the years, advancements in microchip manufacturing and other electronics as a whole have allowed the UAVs to scale down in size. In 1997, Defense Advanced Research Projects Agency (DARPA) facilitated the development of a new class of UAVs referred to as micro air vehicles (MAVs). DARPA initially defined these vehicles as a form of UAV that does not exceed 15 cm (6 in) in any dimension with a mass of less than 100 grams. [3]. The term MAV has been relaxed to include vehicles with a maximum dimension of less than one meter in any direction and mass less than 500 grams [4, 5]. These smaller vehicles typically possess lower noise signatures and radar cross-sections compared to the larger UAVs, and this lower detectability offers numerous advantages.

There are three basic mission types that are identified for MAVs; over the hill reconnaissance, indoor and urban operations, and immersive sensing [3]. A depiction of these mission types are shown in Fig. 1.1. Over the hill reconnaissance is one of the main military use cases where the MAV can be used to extend the line-of-sight of the operator. In this case, MAVs are used to gather information beyond some physical barrier such as forest, hills, or buildings. For indoor

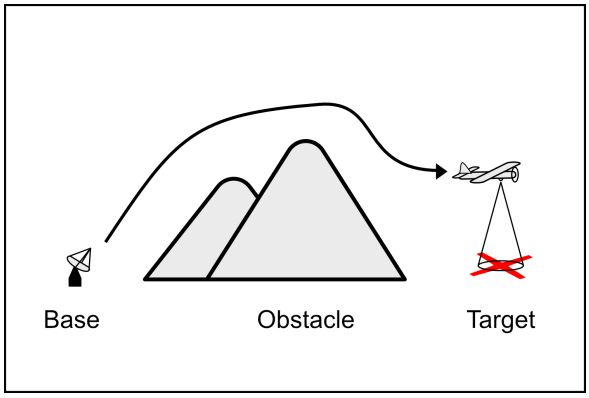

(a) Over-the-hill reconnaissance.

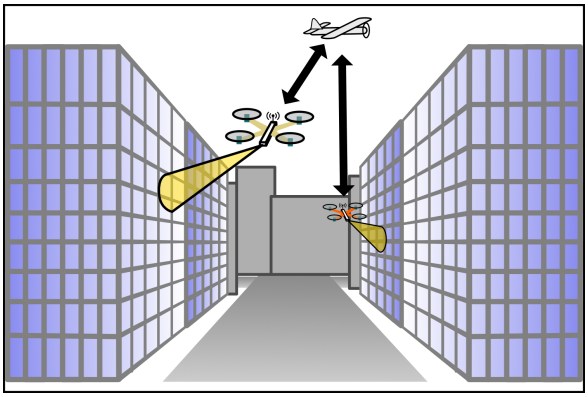

(b) Urban reconnaissance.

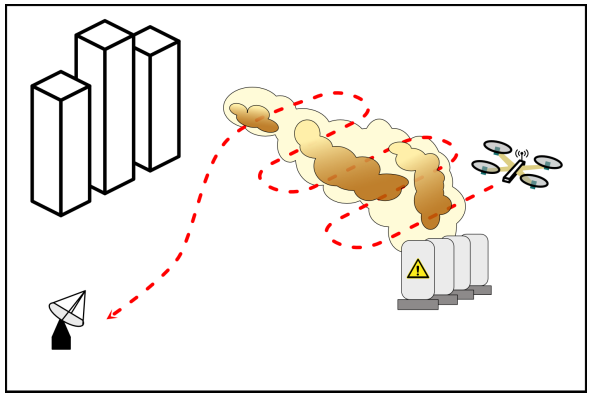

(c) Remote/immersive sensing.

Figure 1.1: Common UAV missions.

and urban operations, MAVs are expected to operate in cluttered environments with many such obstacles. In this situation, MAVs can be much more agile and maneuverable compared to larger UAV performs. Lastly, immersive sensing with MAVs could be accomplished by flying though potentially hazardous environments and collect sensory data. For example, a group of MAVs could fly through chemical clouds and relay information about chemical composition and movement back to a ground operator. These are just a few potential use cases for MAVs; these vehicle could be equipped with a number of different payload for various mission objectives.

1.1.2 Advantages of MAVs

In terms of military applications, MAVs are typically used in applications such as intelligence, surveillance, reconnaissance (ISR), as well as search and rescue missions. The rapid deployment

capability of most MAV systems means that they can be launched at a moments notice and help monitor rapidly changing environmental conditions. A MAV can provide a robust platform for real-time video or other sensor feeds to the ground operator. Moreover, the size and maneuverability of rotary-wing concepts such as helicopters and multi-rotors make them a promising solution for ISR in crowded urban environments. Additionally, the lower production cost of these platforms make them ideal for use in contested environments where recovery of vehicles becomes optional.

The small form factor and mass of MAVs makes them ideal for foot-soldiers to carry. It is conceivable that a single soldier could carry multiple MAVs, which could be used to scout ahead and relay valuable information back to a command center. This could be much faster than waiting on a larger UAV to be deployed from a forward operating base. In another scenario, a larger UAV could be used to identify points of interest for MAVs to examine especially when operating near contested spaces. The smaller size of MAVs makes them harder to detect and accurately target compared to larger UAVs. Despite these advantages, special care must to be taken to ensure that this additional equipment does not over burden personnel because it is added to the 87-127 lbs of gear carried by the typical warfighter [6].

1.1.3 Limitations of Current MAVs

Despite these advantages, MAVs still face many developmental challenges ranging from disturbance rejection and gust tolerance to increased endurance and propulsive efficiency at low Reynolds's numbers. The overall endurance for MAVs is one of the problem areas that prevents the use of MAVs from becoming more wide spread. Some studies have looked at increasing the aerodynamics efficiency of low Reynolds's number ($< 50{,}000$) propellers by optimizing rotor parameters [7–9] . While advances are being made in these fields, it could take years for these systems to see major improvements in these areas.

The altitude, range, and endurance of these predominantly electric platforms are restricted by the low energy density of current battery technology [4, 5, 10]. Over the past few decades, improvements in lithium polymer batteries have made this battery chemistry a popular choice for electric UAV and MAV applications, but the improvement are not enough for MAVs. Limited

battery capacity places more stringent constraints on rotary-wing systems compared to fixed-wing aircraft due to the higher power requirement for hovering flight. Often, rotary-wing MAVs have a hover endurance of less than 20 minutes [4, 5], making it imperative to consider unconventional approaches to improve the effectiveness of hover-capable platforms for ISR missions.

1.2 MAV Range Extension by Proposed Tube-Launch Method

Although directly improving the endurance of rotary-wing MAVs poses a significant challenge, the overall range could be increased by launching the vehicle as a projectile towards the desired target location using a 40 mm grenade launcher. Instead of draining a significant portion of the onboard battery energy to reach the intended altitude and range, the projectile phase of flight would preserve the stored energy until the vehicle reaches its designated operating location. This ensures that the vehicle's stored energy can be fully expended once at a target area in the case of a disposable platform. If the vehicle is intended to be recovered, the energy saved by launch could be used to increase the range for the returning flight. Furthermore, the use of a grenade launcher would take advantage of preexisting hardware that a typical warfighter would be trained to utilize. The ability to leverage existing equipment like a 40mm grenade launcher, would significantly increase the convenience and practical applicability of tube-launched systems.

The projectile launch method offers several other key advantages aside from increasing vehicle range such as ease of deployment and reduction in deployment times. By launching a vehicle directly into the air, a ground operator can deploy the vehicle without locating an unobstructed takeoff area. For example, a multi-rotor may have difficulty taking off from an inclined or rocky area. Moreover, takeoff might have to be aborted if a propeller or rotor were to strike debris near the site. In addition to ease of deployment, a projectile launched vehicle can be rapidly deployed since the flight time between the launch and target location is reduced because the deployment speed is limited by the launch speed rather than the vehicle's maximum velocity. Moreover, while the vehicle travels as a projectile, it will be virtually silent until the rotor deploy just seconds before arriving at the target area [11].

The proposed projectile launch technique can be decomposed into several distinct phases of

flight, which are shown in Fig.1.2. The vehicle begins in a folded state and inserted into the launcher. Once launched, the vehicle enters the projectile or ballistic phase, and soon after, a protective cap is released from the vehicle. The cap is intended to protect the vehicle from the explosive charge used for launch. After the vehicle reaches the apex of the flight path, the rotor system is deployed and the rotors start spinning. If the projectile speed is too large for successful rotor deployment, a drag device such as a parachute could be deployed to slow the vehicle before rotor deployment. Next, the crucial transition from the passive projectile phase to controlled powered descent begins with the application of rotor braking thrust as the vehicle reaches the target attitude and range. Once sufficiently slowed, hovering flight is attained, and the vehicle can perform its desired mission and fly back to the operated if necessary.

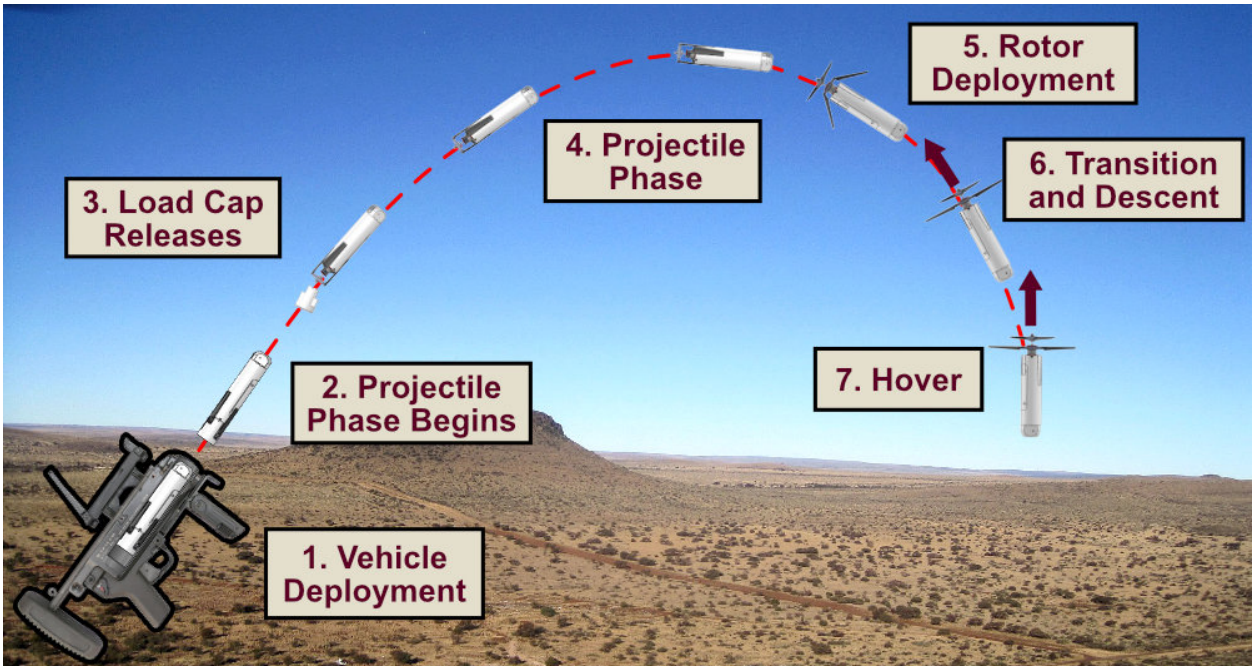

Figure 1.2: Gun-launched MAV concept: Flight phases.

1.3 Previous Tube/Gun-Launched Vehicles

There are currently two different types of tube-launched vehicle at various phases of development; fixed-wing and rotary-wing platforms. Of these platforms, fixed-wing aircraft make up the vast majority of existing tube-launched concepts and many are in production. In contrast, fewer tube-launched, rotary-wing platforms exist and none of them have reached the production phase.

Currently, there are a few different mechanisms for tube-launching (or sometimes referred to as canister-launching) a vehicle. At a fundamental level, the vehicle must be folded to fit within a launcher that propels the vehicle using either an explosive charge or pressurized air. The energy stored in the charge or pressurized air can be converted to kinetic energy to propel the vehicle from the launcher. After the vehicle is released, the vehicle transitions from the folded state to a flying state, and then the vehicle performs its mission.

The most common launch method involves the use of a specialize canister and can be launched from the ground by a single person. These canisters are normally slightly larger than the vehicle itself and can be easily transported. Recently, defense companies like Raytheon have tested a variation on the canister launch method by mounting an array of canisters to a ground vehicle or trailer under a navy sponsored program called LOCUST [12]. Multiple vehicles can be launched near simultaneously creating a swarm of UAVs, which can be difficult for an adversary to target and destroy each vehicle.

Recently, tube-launched vehicles were taken to new heights, whereby the UAV is ejected from another vehicle. UAVs have been successfully deployed from airplanes, helicopters, ships, and even submarines. In most cases, the UAV is released from its mother-ship while still contained within a canister. When deployed from an airplane or helicopter, the canister is released from the aircraft, and a parachute is used to slow the descent of the canister. The UAV is then deployed from the canister to perform its mission. Similar to the previously mentioned LOCUST concept, UAV canisters have also been tested on ship based platforms. When deployed from a submarine, the canister rises to surface of the water, and then the vehicle is fired into the air as in the case of Lockheed Martin's Outrider and AeroVironment's Blackwing [13, 14].

1.3.1 Fixed-Wing aircraft

There are a few existing military platforms that take advantage of a projectile flight phase to conserve onboard energy or to facilitate rapid deployment; however, most of these are fixed-wing platforms such as Raytheon's Coyote [12] and AeroVironment's Switchblade [15]. In the case of the Switchblade and the Coyote, the main purpose of tube launching is for ease of deployment. Once launched, the wings and control surfaces are unfolded, and the vehicle begins its mission. Both of these systems can be used for surveillance, but are often equipped with explosives and used to strike targets. Vehicles with strike capabilities are sometimes referred to as loitering munitions. Table 1.1 shows the gross takeoff weight, wingspan, endurance, and range specifications for several tube-launched, fixed-wing UAVs.

Platform	GTOW [kg]	Wingspan [m]	Endurance [min]	Range [km]
Blackwing [13]	1.8	0.69	-	-
Coyote [12]	5.9	1.47	60+	80
Hero-250 [16]	25.0	-	180	150
Outrider [14]	1.7	≈ 1.2	120+	40
Switchblade [15]	2.5	0.61	15	10

Table 1.1: Specifications of tube-launched fixed-wing UAVs

The most notable feature of the fixed-wing concepts listed in Table 1.1 is the endurance of these systems. Although the fixed-wing platforms tend to have higher endurance compared to the rotary-wing ones, fixed-wing vehicles struggle to focus on a single target for an extended duration or navigate in confined spaces. Moreover, current tube-launched fixed-wing systems are at least an order of magnitude larger in terms of both mass and size to meet the definition of a MAV.

1.3.2 Rotary-Wing aircraft

In recent years, the development of hover capable, tube-launched platforms have begun to emerge such as the Streamlined Quick Unfolding Investigation Drone (SQUID) [17, 18] developed

Figure 1.3: Raytheon's Coyote version used for hurricane hunting [1].

by Caltech and the gun-launched MAV (GLMAV) [11, 19–22] developed by the French-German Research Institute at Saint Louis. The focus of this study is based on the Tube-Launched MAV (TLMAV) developed at Texas A&M University [23, 24]. A size comparison of these platforms can be seen in Fig. 1.4. Unlike the previously mentioned fixed-wing UAVs, both of these platforms are still within the prototyping phase and may not be widely used for years.

The SQUID is a ballistically launched quad-copter that can be fired from a moving platform. The vehicle has a folded diameter of 83 mm (3.26 in) and a mass of 530 g. The SQUID is launched using a pneumatic cannons with an exit velocity of 15 m/s (49 ft/s). The developers of the system sought to create a reliable vehicle deployment strategy that could also be used to extend the range of the vehicle. The arms of the quad-copter that hold the motors and propellers are folded into the main body, and the arms are passively unfolded after launch using a nichrome wire release

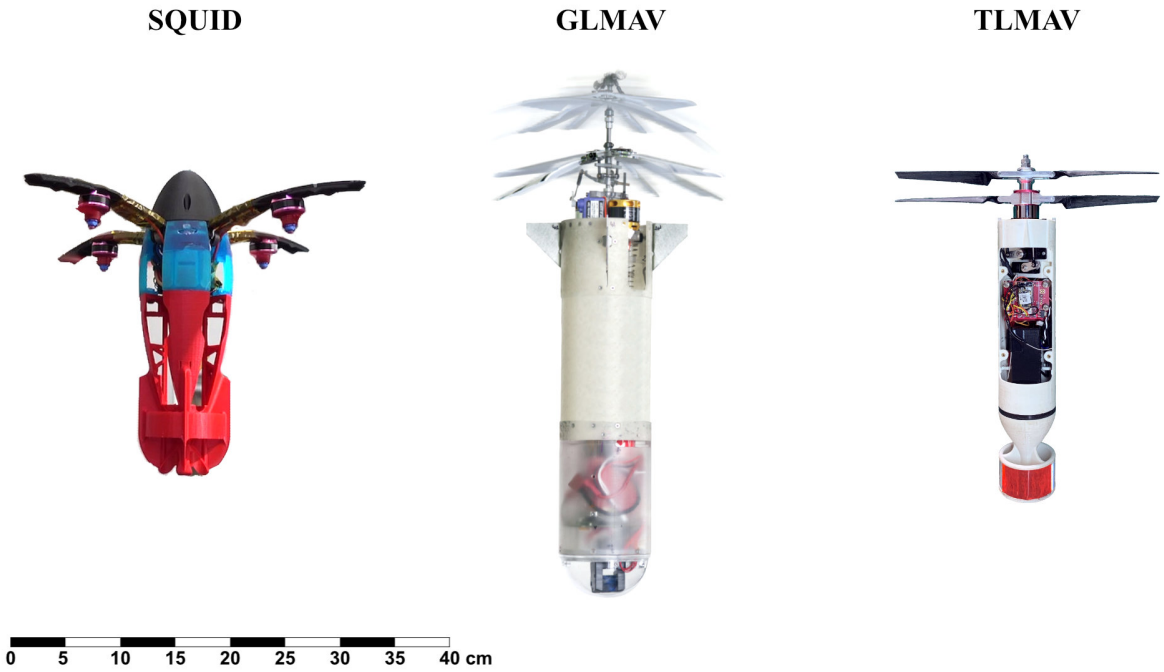

Figure 1.4: Size comparison of current tube-launch systems.

mechanism. Additionally, a study demonstrated that the vehicle could be launched from a platform moving at speeds up to 22 m/s (50 mph), and the vehicle's control system could stabilize the vehicle after launch [17]. Currently, the researchers are developing a larger 3.3 kg vehicle equipped with a suite of sensor to automate the launch and stabilization systems [18].

On the other hand, the GLMAV concept is a significantly larger coaxial rotary-wing design that was designed with the goal of range extension. It has a folded diameter of 80 mm (3.15 in) and a total mass of 1.05 kg. The vehicle is fired from a custom mortar launcher that weighs 10 kg and is 1 m (3.04 ft) in length. The launcher is capable of projecting the fin-stabilized vehicle over 500 m (1640 ft) in range and to an altitude up to 100 m (328 ft). After the apex of flight, the coaxial rotor system is deployed from the vehicle, and the rotor thrust decelerates the vehicle as it approaches the target range of 100 or 500 m. The GLMAV is equipped with a single camera in the nose of the vehicle used for scene observations that is live-steamed back to the ground operator. The camera view is split using a prism to allow the single camera to simultaneously observe in front and below

the vehicle. The vehicle only possesses enough battery capacity to fly for about five minutes and can be reused if recovered. As of 2017, a demonstration of the transition from ballistic flight to hover has not been shown, but projectile launch stability and vehicle stability in hovering flight have been revealed [11].

1.4 Current Research

1.4.1 Research Objective

The ultimate goal of this work is develop a hover-capable MAV that can be rapidly deployed using a 40 mm grenade launcher to extend the overall range of the vehicle. However, the scope of the present work was limited to developing a larger 52 mm outer diameter platform to serve as a testbed for a future 40 mm system. The decision to design a larger system was primarily made to take advantage of a wider selection of commercial-off-the-shelf (COTS) parts. Despite the larger size, the first objective is to develop a scalable design using available hardware and eventually scale the design back to the initial 40 mm constraint. The overall design should be mechanically simple and robust to the impulsive force experienced during launch. A number of different vehicle configurations were considered, but ultimately a coaxial rotor system was chosen.

The second objective is to build a proof of concept vehicle capable of being launched as a projectile. The prototype was constructed using primarily COTS parts and rapidly prototype parts. A compact and simplified electrical and mechanical control system had to implemented and proven. Additionally, a custom pneumatic cannon was built to serve as the launcher for ballistic testing to demonstrate the capabilities of vehicle.

The third objective involves performing systematic experiments to show the capabilities of the vehicle and flight controller to handle the various phase of flight depicted in Fig. 1.2. Wind tunnel tests and targeted flight tests were devised to observe the vehicle response to these various flight conditions. These tests were also used as an opportunity to tune the flight controller used to stabilize the system in the different flight regimes.

A fourth and final objective is to demonstrate a vertical ballistic launch and vehicle recovery

which is a stepping-stone to performing the full mission. The vertical launch can be view as a special case of a typical parabolic ballistic launch with an angle near 90 degrees measured from the horizon. The rotors are deployed at the apex of the flight path while the axial descent speed is low. A successful vertical launch recovery represents a major milestone in the development of a tube-launched system for range extension.

1.4.2 Technical Barriers

The overarching goal of this research effort is to develop a coaxial rotor based MAV that could be launched from a grenade launcher. However, developing this platform presents some key technical barriers which stem from scaling the vehicle down to fit within the barrel of a grenade launcher, which has an inner diameter of 40 mm, in-flight reconfiguration (passive rotor deployment from a folded state), and the complex dynamics experienced during the transition from projectile to hovering mode. Some specific challenges include (1) designing and building a compact rotorcraft with outer diameter less than 40 mm, (2) foldable coaxial rotor blades with passive unfolding strategies which avoid rotor collision, (3) simplified and compact swashplateless pitch, roll and yaw control strategies, (4) ultralight-weight autopilot with small footprint, (5) ability to handle the high accelerations of an explosive take-off, (6) passive and active control strategies ensuring stable attitude dynamics in flight, especially during the transition from the projectile mode to the hovering helicopter mode, (7) understanding and improving the controllability and disturbance rejection (gust tolerance) of the vehicle in hover for improved robustness in adverse conditions, and (8) optimizing the rotor-motor-ESC (electronic speed controller) combination to achieve a hover endurance of at least 30 minutes.

The platform's compactness and in-flight reconfiguration and transition requirements necessitate a multifaceted approach to the vehicle design. This study will mainly focus on overcoming the second through seventh barriers listed above by developing a coaxial rotor based MAV controlled via thrust vectoring and capable of stable hovering. To facilitate development, the size constraint was slightly relaxed and an intermediate prototype was developed. The intermediate model had an outer diameter of 52 mm instead of the required 40 mm diameter. Future iterations will miniaturize

this intermediate prototype by optimizing and scaling the components for the final 40 mm design. The objective of the present study was to enable the vehicle to achieve a stable projectile phase, deploy the rotors, and then successful transition from the projectile phase to a stable hover, following a vertical launch. This required many innovations in the vehicle design, rotor deployment mechanism, controls system, and systematic flight testing, which are discussed in this thesis.

1.4.3 Contributions of the Present Research

The key contributions of this research include:

1. Designed, built, and flight-tested the world's smallest tube-launched hover-capable MAV.

2. Developed a mechanically simple strategy for pitch and roll control using a two-axis gimballed thrust-vectoring mechanism. The gimballed design was in place of a swashplate used on traditional helicopters.

3. Designed and prototyped a rotor based on previous MAV-scale rotor design studies. Initial single rotor experiments showed that the rotor design can reach a Figure of Merit of up to 0.5.

4. Demonstrated that a passive rotor start-up technique could be used to deploy the rotors in flight using centrifugal force and a time delay between spinning up the upper and lower rotors.

5. Performed wind tunnel experiments to demonstrate that the thrust-vectoring mechanism combined with a cascaded PID feedback controller can stabilize and reject wind disturbances. Wind tunnel experiments showed that the controller can stabilize the MAV during the powered descent phase.

1.5 Organization of Thesis

This thesis consists of 10 chapters that show the gradual development of a tube-launched MAV to meets the aforementioned objectives. In Chapter 1, the background and motivation for the

development of MAVs is established. The limitation of current technology that impacts the overall range and endurance of MAV platforms is discussed, which leads to the need to consider a novel approach to address the problem without relying on advances in battery technology. The idea of launching a MAV to a desired altitude and range range is proposed to preserve onboard energy storage to maximize time at target location. Previous tube-launched vehicles vehicle are discussed, and requirements for a new hover-capable vehicle is explored.

In Chapter 2, the vehicle configuration selection was discussed in the context of the vehicle design requirements. The hover-capable vehicle platforms considered for this project included multi-rotors, single rotor helicopter, coaxial helicopter, and tandem helicopter designs. Ultimately, the coaxial helicopter configuration was selected primarily based on the compactness design requirement. Additionally, an overview of the vertical and ballistic launch vehicle designs are presented. This includes a discussion about the relative placement of the AC and CG for the respective design variations. The major components of both vehicle designs are introduced.

In Chapter 3, the selection a flight control strategy for the coaxial rotor system was explored. Two different strategies, a swashplate mechanism and a thrust-vectoring mechanism were considered. The thrust-vectoring mechanism, which provides pitch and roll control, was ultimately chosen based on the simplicity of design and implementation. Different variations of the mechanism design were also explored, but a single, dual-axis gimbal with the propulsion system mounted to the inner gimbal was chosen. To further simplify the design, a specialized coaxial motor unit was selected for the propulsion system due to its overall compactness.

In Chapter 4, details of propulsion subsystem including the folding rotors and the coaxial motor unit are discussed. The rotor parameters were selected based on previous MAV rotor design studies and constraints placed on the overall design. The singe and coaxial rotor performance were measured on a hover stand to ensure the rotors were capable of producing sufficient thrust, and the results are also discussed.

In Chapter 5, the avionics systems are described, which consists of an autopilot, telemetry module, serial receiver, and transmitter. The autopilot selected for the vehicle is discussed along

with its capabilities. The communications systems between the autopilot, ground station, and pilot are also presented. The chapter concludes with the description of the flight control system and rotor start-up sequence implementation on the autopilot.

In Chapter 6, an overview of the fuselage and fin assembly design is shown. The fuselage forms the structural backbone of the vehicle, and it houses all the subsystems. The manufacturing process for the fuselage and fin assembly is also described in this chapter. The purpose of the fin assembly is to lower the aerodynamic center with respect to the center of gravity to improve stability in the vertical launch configuration.

Chapter 7 discusses the systematic wind tunnel experiments performed with the vehicle placed on a single degree-of-freedom stand. The experiments were intended to replicate conditions such as forward flight and axial descent in a controlled environment. These tests were also used to tune the pitch feedback controller and to show that the controller could reject the disturbances. The vehicle's response to these disturbances is included in this chapter.

In Chapter 8, the free flight testing is discussed. The flight testing procedures and flight test data from the first set of indoor hovering flight tests is presented. The axial descent tests were repeated with the vehicle in free flight to determine the ability of the controller to stabilize the vehicle in that adverse condition. The results of a successful test are included and discussed.

In Chapter 9, the details of the vertical launch tests that were performed with a dummy and later with the vehicle are discussed. The dummy with the similar inertial properties to the vehicle was vertically launched from a pneumatic cannon, and the response of the autopilot was recorded. Finally, a vertical launch with the vehicle was performed, and the vehicle was able to transition to free flight after launch. The flight test data from the successful launches are presented.

In Chapter 10, a summary of the present work and key conclusions for this study are included. Recommendations for future research on the tube-launched MAV is presented. This include a set of proposed steps and developmental milestone towards the development of a viable tube-launched platform.

2. VEHICLE DESIGN OVERVIEW

2.1 Configuration Selection

The current design was driven by a set of requirements, especially, the spatial constraints imposed by the 40mm (1.6in) grenade launcher, which drove the majority of the design decisions for the overall configuration. The secondary requirement was that the configuration should be capable of hovering flight in moderate wind conditions. Other considerations included overall system efficiency, agility, and ease of packing. After considering all of these factors, a coaxial helicopter configuration was ultimately chosen as a basic for the vehicle design.

Exclusively hover-capable vehicle types were considered for the tube-launched platform design. Configurations that were examined included multi-rotor, single rotor helicopter, coaxial helicopter, and tandem helicopter designs. While hybrid multi-rotor/fixed-wing designs could significantly increase overall endurance in fixed-wing flight, they were not considered due to the additionally complexity of packaging such a system into a limited footprint.

Due to the increasing popularity and simplicity, a multi-rotor configuration was heavily considered. The lack of a powertrain or transmission and few moving parts are desirable characteristics for a creating a mechanically robust vehicle by minimizing the number of points of failure. At MAV scales, multi-rotors can be very agile and maneuverable according to scaling law [10, 25].

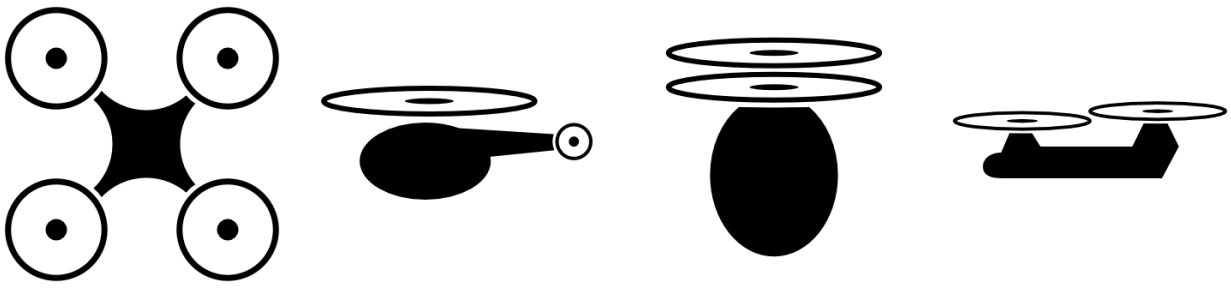

(a) Multi-rotor. (b) Traditional helicopter. (c) Coaxial helicopter. (d) Tandem helicopter.

Figure 2.1: Vehicle configurations considered for tube-launched vehicle.

However, the internal space and additional complexity required to integrate folding and deployable arms attach the motors would likely take up too much internal volume. Additionally, the maximum rotor diameter would be much more limited compared to the other configurations, and the higher rotor disc loading would mean increase the power requirements of the vehicle. A higher power requirement directly translate to lower endurance for the system. For these reasons, the multi-rotor configuration was not selected.

The next set of design configurations considered for this application consists of single rotor helicopter, coaxial helicopter, and tandem helicopter designs. In general, all of these designs are more mechanically complex in terms of the number of move parts compared to a multi-rotor. The additional complexity is derived from the swashplate (Fig. 2.2) that is used to control the pitch of the blades as they rotate to generate control moments. However, these systems are capable of using larger diameter rotors compared to multi-rotor of the same footprint which means the disk loading is reduced and will the decrease the power needed for hovering flight. Of the different helicopter configurations, the coaxial helicopter will have lowest disk loading for the same footprint. An additional benefit of lower disk loading is related to overall rotor noise reduction, so the lower acoustic signature would make the vehicle harder to detect [26].

Of the traditional helicopter configurations, the coaxial design seems to be the apparent choice for this vehicle design. In terms of compactness, the most stringent of the design constraints, the coaxial configuration also benefits from a more compact yaw control mechanism by balancing the torque produced by the counter rotating rotors, whereas a traditional single rotor helicopter requires a tail boom and a tail rotor, which need to be folded leading to significant complexity. Also, because the tail rotor is not contributing significantly to the vertical thrust components, it reduces the energy available for hovering and forward flight, as opposed to a coaxial rotor system where both rotors contribute to the vertical thrust. The tandem design also does not lend itself to a compact design because the spacing of the separate rotor system severely limits the maximum rotor diameter similar to the multi-rotor for a given footprint. In a technical design report for a similar vehicle by Wereley and Pines [25] it was determined that a coaxial rotor system was

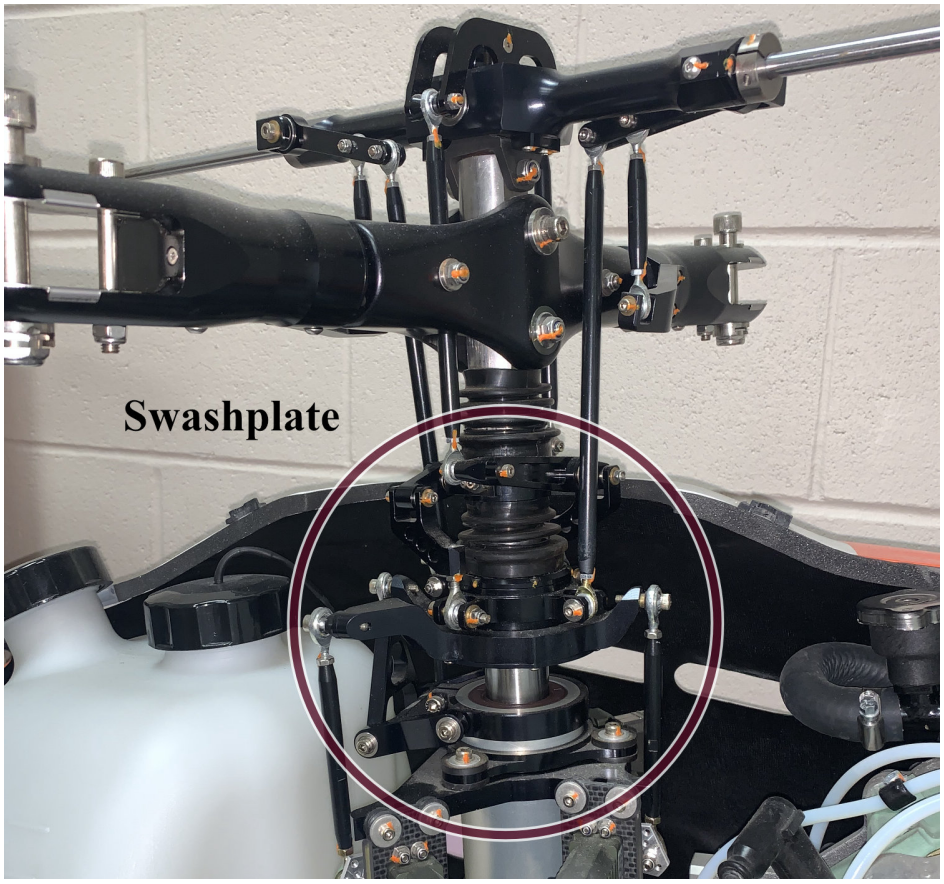

Figure 2.2: Example of helicopter swashplate with full cyclic and collective control.

a better candidate for a tube-launched rotorcraft. This assessment was based on factors such as efficiency, folding compactness, and ease of packaging.

For the coaxial design to be more advantageous compared to a multi-rotor, the overall mechanical complexity needed to be reduced. As previously mentioned, the helicopter swashplate is a major source of mechanical complexity, especially for coaxial rotor system where two set of mechanically linked swashplates are often used for control. The study by Wereley and Pines looked at alternative control mechanisms such as control fins or a gimballed rotor system, which made the coaxial configuration of the design [25] more desirable compared other designs. The simplifications for the controller system will be further discussed in the next chapter. Moreover, the cylindrical outer-body-shape constraint imposed by the launcher, a coaxial helicopter configuration became the natural choice because a cylindrical shell could be used as the body and the rotor

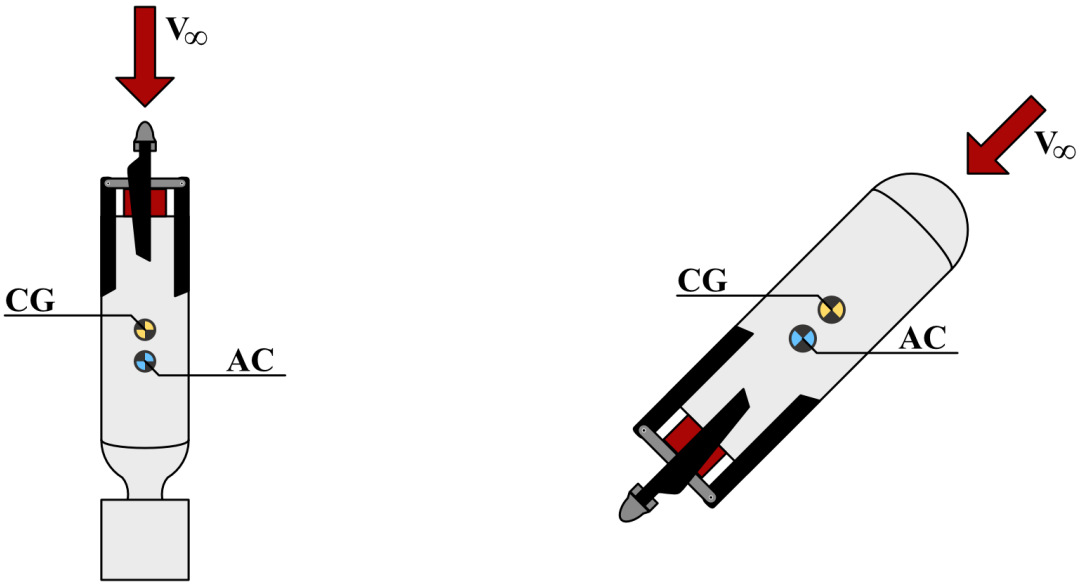

(a) Vertical launch configuration.

(b) Ballistic launch configuration.

Figure 2.3: AC and CG placement for ballistic and vertical launch configurations for passive stability. Configurations are shown oriented with respect to vehicle launch directions and resulting freestream velocities.

blades could be easily folded against the body.

2.2 Vehicle Launch Configurations

Two different vehicle designed were used for the purposes of this study: (1) the vertical launch configuration, and (2) the ballistic launch configuration. Both vehicle designs are fundamentally the same in terms of basic internal layout and share common subsystems. An external view of the two layouts are depicted in Fig. 2.3. The vertical launch design represent an intermediate prototype used to test various subsystem in more ideal conditions that will be discussed later. The ballistic launch vehicle is more representative of the layout for the future 40 mm grenade-launched system.

2.2.1 Vertical Launch

The vertical launch platform is intended as a stepping-stone towards the ultimate goal of developing a rapidly deployable, tube-launched vehicle. By launching the system vertically, the rotor deployment sequence and control system can be tested at low axial descent speeds to gain confi-

Table 2.1: Weight breakdown of the vertical launch vehicle.

Components	Mass (g)	% Total
Propeller and Hubs	22	6.0
Motor	62	16.9
Fuselage	72	19.7
Battery	102	27.9
Electronics	34	9.3
Servo Actuators	25	6.8
Two Axis Gimbal	9	2.5
Fin Assembly	40	10.9
Total	366 g	100.0 %

dence in the system under near ideal conditions. The rotor system and control systems are then triggered as the vehicle reaches the apex of flight. This version is slightly different from the ballistic version due to differences in passive stability requirements. The weight breakdown for the vertical launch system can be viewed in Table 2.1.

The vehicle is inserted into the launcher with the rotors system oriented to the launcher outlet. In this configuration, the CG must be ahead of the AC to ensure that the vehicle is passively during the projectile phase as shown in Fig. 2.3a. The addition of the radial fin assembly to the lower portion of the vehicle, brings the AC down below the CG. The fins can stabilize the vehicle between launch and some point near the apex, but the effectiveness of the fins will decrease as the vertical velocity goes to zero. Since the rotor system will be deployed near the apex of flight, the fin is only used to augment the aerodynamics stability up to that point. The flight control system is responsible for maintaining vehicle stability after rotor deployment.

2.2.2 Ballistic Launch

The ballistic launch configuration is likely more representative of the final vehicle design that will be launched from the 40 mm grenade launcher. In place of the fin assembly, attached to the lower portion of the vehicle in the vertical launch configuration, an aerodynamic nose cap is secured in its place as seem in Fig. 2.3b. The internal layout of the vehicle is exactly the same as the vertical launch configuration. The weight breakdown for the ballistic launch system can be

Table 2.2: Weight breakdown of the ballistic launch vehicle.

Components	Mass (g)	% Total
Propeller and Hubs	22	6.4
Motor	62	18.1
Fuselage	72	21.1
Battery	102	29.8
Electronics	34	9.9
Servo Actuators	25	7.3
Two Axis Gimbal	9	2.6
Nose Cap	16	4.7
Total	342 g	100.0 %

viewed in Table 2.2.

In the ballistic configuration, the vehicle is inserted into the launcher with the nose cap facing the launcher outlet. To maintain passive aerodynamics stability during ballistic flight, the CG must be position closer to the nose cap with the AC closer to the rotor system as shown in Fig. 2.3b. Depending on the final positioning of the AC and CG, a set of deployable fins could be added to the upper part of vehicle fuselage in enhance the passive stability of the system. In addition to passive stability, the AC and CG positioning will automatically ensure that the rotor system is pointed skyward near the end of the ballistic flight path when the rotors are deployed. The rotor thrust can immediately begin slowing the vehicle without expending much control effort to reorient the system for the braking maneuver.

2.2.3 Common Vehicle Subsystems

The internal component layout of the two vehicle configurations are identical. The layout of the vertical launch configuration can be viewed in Fig. 2.4, and the ballistic launch configuration can be seen in Fig. 2.5. In both figures, the major components are highlighted.

The major subsystems common to both vehicle configurations includes the thrust-vectoring mechanism, propulsion system, avionics, battery, and fuselage assembly. The thrust-vectoring mechanism enables pitch and roll control using a two-axis gimbal driven by two independent servo actuators. Control moments are created by offsetting the thrust axis from the CG. The propulsion

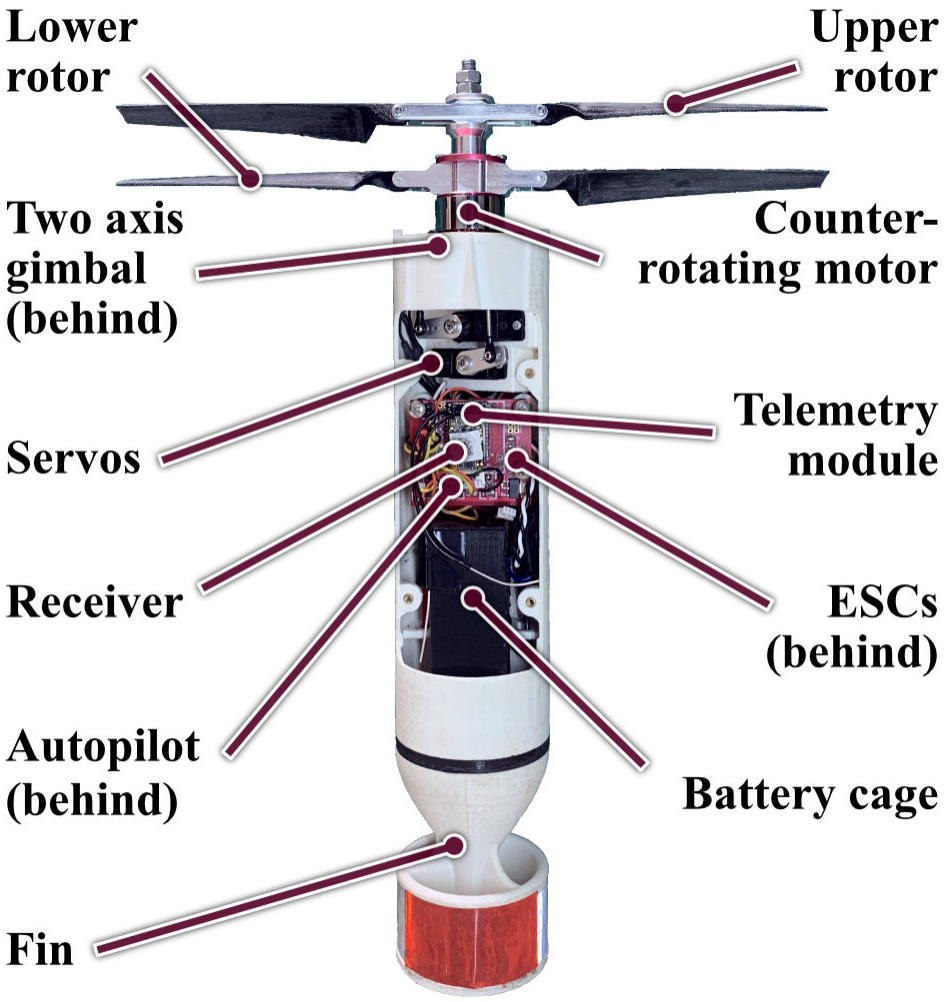

Figure 2.4: Vertical, tube-launched MAV layout.

system consists of the coaxial motor unit, electronic speed controllers (ESCs), and counter-rotating, folding rotors. The rotors and motor unit produces thrust and yaw control using collective and differential rpm control, respectively. The avionics system is comprised of the autopilot, receiver and telemetry module. The autopilot obtains pilot commands from the receivers, and the commands are relayed to the feedback controller. Actuator and motor command are also sent by the autopilot, and flight telemetry is sent via the wireless communication module to a ground station. All of the vehicle subsystem are powered by a 3-cell, lithium polymer battery housed in lower section of the vehicle. The subsystems of the vehicle are encased and fastened to various mounting locations

within the fuselage. The following chapters will discuss the major subsystems in further detail.

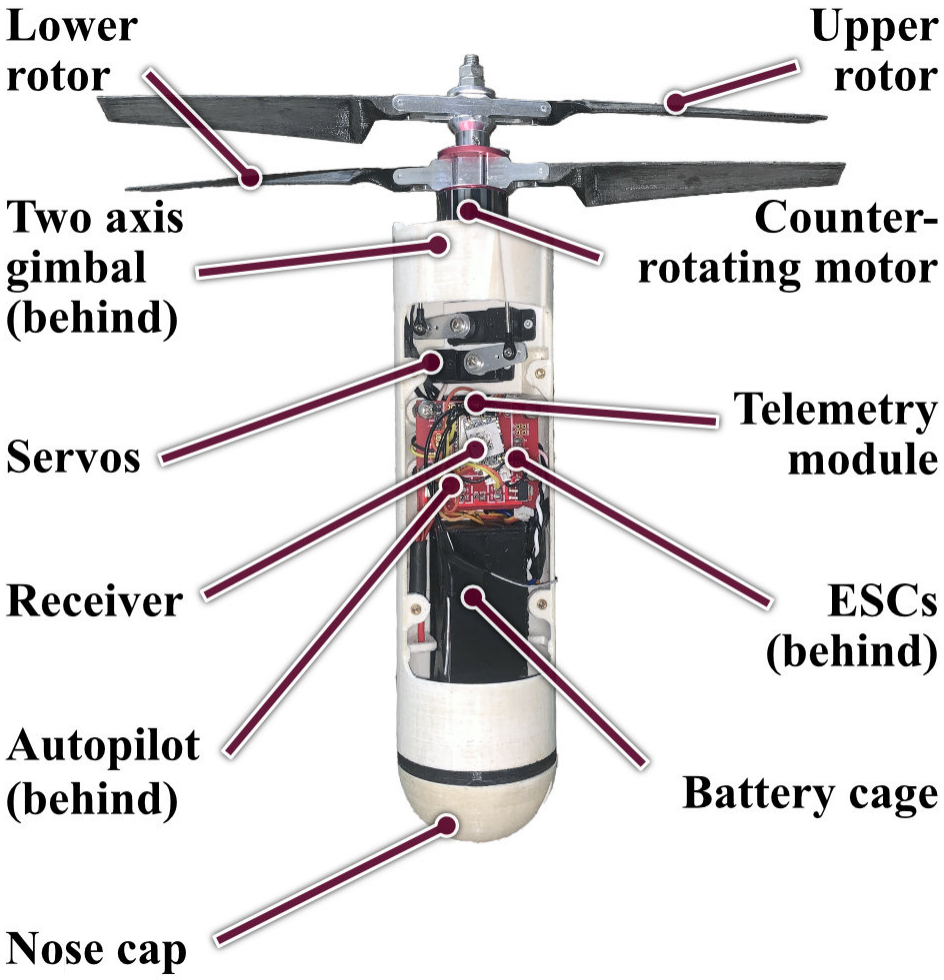

Figure 2.5: Ballistic, tube-launched MAV layout.

3. THRUST-VECTORING MECHANISM

3.1 Selection of a Control Mechanism

The control mechanism for pitch and roll control needed to be compact and reliable, and therefore, the selection of the mechanism was based on that criteria. Typically, a complex swashplate mechanism is used to generate the control moments to maneuver helicopters. An alternative thrust-vectoring mechanism was considered and implemented on the present vehicle because of its reduced mechanical complexity compared to a swashplate.

In a system with a swashplate, pitch and roll moments are created by changing the pitch of the rotor blades cyclically once per revolution. Blade cyclic pitching is accomplished via tilting the swashplate using a servo actuator. To gain full cyclic and collective control, three servo actuators are required. In the case of a coaxial helicopter, two mechanically linked swashplate can be used, but many MAV-scale coaxial helicopters such as the GLMAV use a single swashplate for cyclic control on the lower rotor and a flybar on the upper rotor to add gyroscopic stability [11]. For the current tube-launched vehicle, a less mechanically complex system was envisioned.

A thrust-vectoring mechanism was considered to be more more reliable for the tube-launched vehicle due to its lower order of mechanical complexity. This reduced complexity should improve the overall reliability of the system when subjected to launch accelerations because there are fewer points of failure. Two different types of gimbal mechanisms were examined; a set of two single-axis gimbals located on opposite ends of the vehicle and one dual-axis gimbal located on one end. For the single axis gimbals, each gimbal would be actuated by a single servo and provide either pitch or roll control. A single motor would be positioned at the center of each gimbal ring, and the motors would spin in opposite directions to provide yaw control. However, the use of two separate gimbal systems would consume more internal volume than a single dual-axis gimbal. Moreover, it will only produce half the control moment that can be generated by tilting both the rotors. Initially, the dual-axis appeared more complex because it required the use of concentric transmission system

powered by two independent motors. The reduction in complexity was enabled by a specialized coaxial motor unit that will be discussed in the next chapter.

3.2 Thrust-vectoring Mechanism

Pitch and roll control is implemented by tilting the rotor plane, which creates pitch and roll moments about the center of gravity (CG) of the vehicle, located below the rotor plane. This is mechanically accomplished by mounting the motor-rotor assembly at the center of a two axis gimbal as illustrated in Fig. 3.1. The mechanism consists of a dual-axis gimbal, two servo actuators, control rods, and motor-rotor assembly.

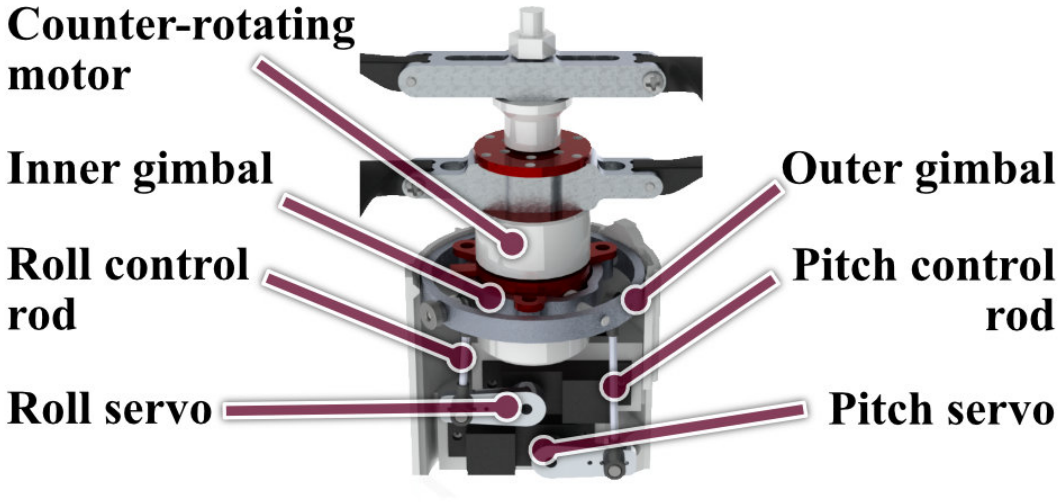

Figure 3.1: Dual-axis gimbal system for thrust-vectoring.

The dual-axis gimbal consists of two concentric aluminum rings joined by shoulder screws that allow one ring to rotate orthogonally with respect to the other. A close up of the gimbal rings are shown in Fig. 3.2. The inner gimbal ring has two holes on either side to form the roll axis, and a pair of shoulder screws are secured to the tapped holes in the inside of the outer gimbal. Similar to the inner ring, the outer gimbal ring has a set of holes at a 90 degrees phase offset from the roll axis to form the pitch axis. The rotation of the motor-rotor assembly about the pitch and roll axes is

actuated by two separate MKS DS6100 servos through control rods with rod-end bearings on both ends. It is important to note that the placement of the rod-end on the inner gimbal at 90 degrees from the roll axis means that pitch and roll are decoupled from each other.

The combination of the double gimbal with the servo mechanism allows the thrust vector, which normally passes through the CG, to be pointed forward/aft (pitch control) or left/right (roll control), similar to a teetering rotor. This tilt of thrust vector creates moments about the CG that cause the vehicle to rotate and translate in a desired direction. The maximum tilt angle of 30 degree in either pitch or roll is limited to prevent the lower rotor from impacting the body. The maximum tilt angle could be increased by offsetting the motor-rotor assembly further from the fuselage, but the servos would have to produce more torque to actuate the gimbals.

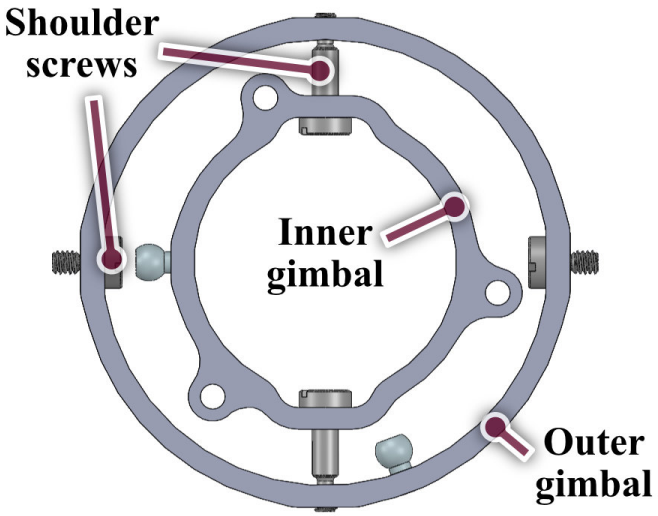

Figure 3.2: Close-up of the two axis gimbal.

4. PROPULSION SYSTEM

The propulsion subsystem consists of the coaxial motor unit, folding rotors, and electronic speed controllers (ESCs). The motor was selected for its thrust producing capabilities and compact design. The folding rotors were custom designed for the vehicle. The COTS ESCs were selected based on the motor specifications. The entire propulsion was tested on a custom hover stand to ensure that the system produced sufficient thrust for the vehicle.

4.1 Coaxial Motor Unit

The overall complexity of the thrust-vectoring mechanism was greatly reduced by utilizing a specialized counter-rotating motor for the vehicle. The motor unit eliminated the need for a transmission to drive the rotors, and direct drive systems tend to be more compact. This allow each rotor to be directly and independently driven.

The motor unit consists of two brushless DC motors with windings mounted to a common body as shown in Fig. 4.1. The lower motor drives the upper rotor, while conversely, the upper motor drives the lower rotor. A steel shaft connects the lower motor to the upper rotor while bypassing the upper motor. The connecting shaft is isolated from the upper motor by a set of bearings. On the other hand, the upper motor directly drives the lower rotor and is bolted to the upper motor casing. Mechanically decoupling the two motors in this manner allows the propellers to rotate independently and provides separate interfaces for the ESCs. Additionally, the independent control of the motors allows for yaw control through differential rpm of the fixed-pitch rotors.

The particular motor unit chosen for the vehicle was one of a limited selection of COTS motors of the unique coaxial configuration. Selection was based on size and thrust producing capability. The motor had to fit within the inner gimbal of the thrust-vectoring mechanism, which was limited to a motor diameter of less than 25 mm (1.0 in). The vehicle weight was estimated to be about 2.9 newtons (0.65 lbs.), so the motor-rotor combination needed to at least produce thrust equal to twice the vehicle weight to ensure sufficient control and rotor braking thrust to decelerate the

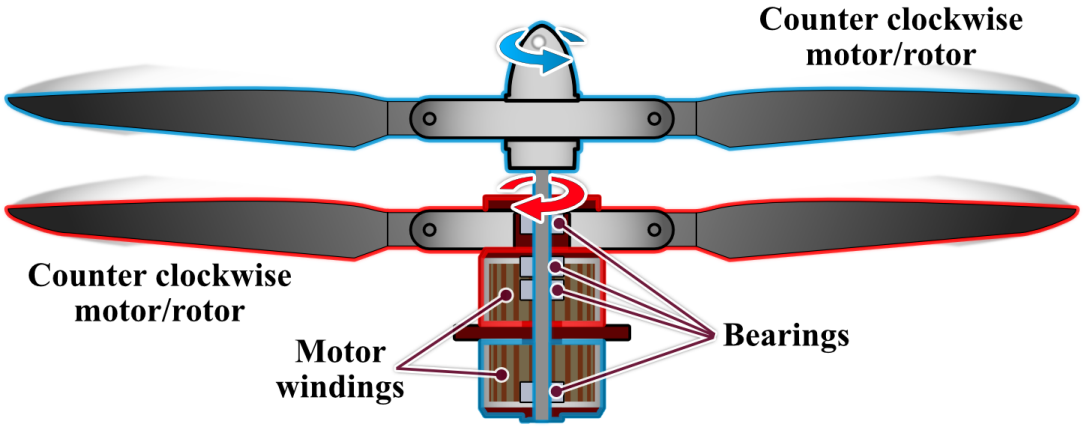

Figure 4.1: Counter-rotating motor unit.

vehicle to hover from the projectile phase. A 1550 kV motor unit was selected for its 23 mm (0.9 in) diameter and ability to produced up to 7.8 newtons (1.76 lbs.) of combined thrust [27].

4.2 Electronic Speed Controllers (ESCs)

The ESCs are responsible for controlling the rotational speed of each of the motors. Each motor is controlled by a single ESC using a pulse width modulation (PWM) signal at a frequency of 500 Hz sent from the autopilot. The output of the ESC is connected to the three different phases of the motor, and the motor speed is controlled by energizing the three phases in a particular sequence creating a rotating magnetic field [28]. The direction of the motor can be reversed by swapping any two the three ESC outputs or changing the order that the phases are triggered.

The ESCs for the vehicle were sized primarily based on the motor specifications. According to the motor manufacturer, 25 amp ESCs were recommended for each motor [27]. For additional safety and because of the negligible differences in size and mass, 35 amp ESCs were used on the vehicle.

4.3 Folding Rotor Design

Another key component of the vehicle design is the pair of counter-rotating folding rotors, which were designed to conform to the body of the vehicle when folded. A number of COTS

folding rotors exist, but it was determined that a COTS solution would take up too much valuable internal space. Since the rotor blades needed to fold against the body, a circular-cambered airfoil was chosen to reduce the volume taken-up by the slots for the blades. This also allowed the blades to be concentric with the body when folded as seen in Fig. 4.2. Moreover, thin, circular camber airfoils have been shown to be more efficient for MAV scale rotors operating at low Reynolds numbers [8, 29].

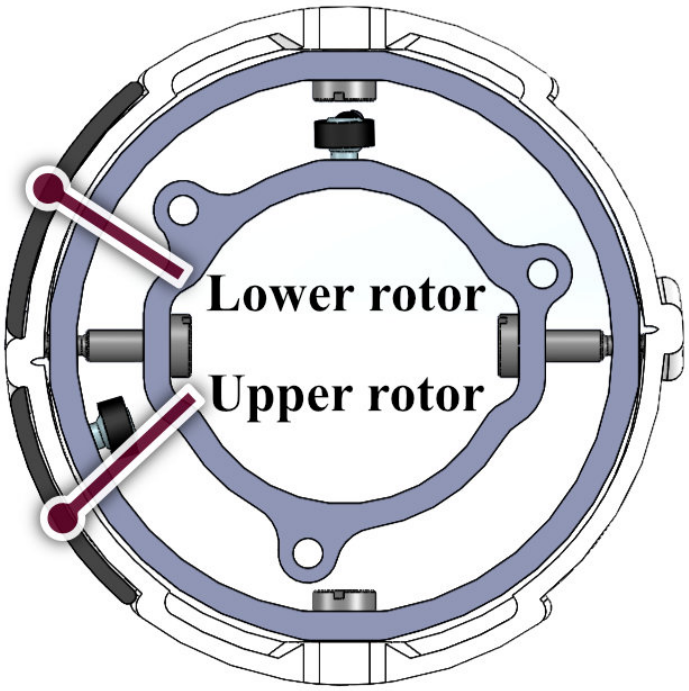

Figure 4.2: The rotor airfoil conforms to the body.

The outer diameter of the rotor in the folded configuration is 51.5 mm (2.03 in), which is equal to vehicle body diameter. The diameter of the rotors, when fully unfolded is 228.6 mm (9 in). The propellers are folded into the body using a flap hinge that is formed between the root of rotor and the rotor hub as illustrated in Fig. 4.3. The hinge consists of a screw that passes though one side of the rotor hub into a hole in the root of the blade, connecting to a tapped hole on the other side of the

rotor. The screw can be tightened with enough friction to prevent the rotors from freely flapping, and a mechanical stopper also exists on the hub to limit the flapwise rotation to 90 degrees while unfolding. The other parameters such as blade twist, pitch angle at 75% span location, and radius, which are listed in the table below, were based on an optimized MAV-scale rotor design [7, 29].

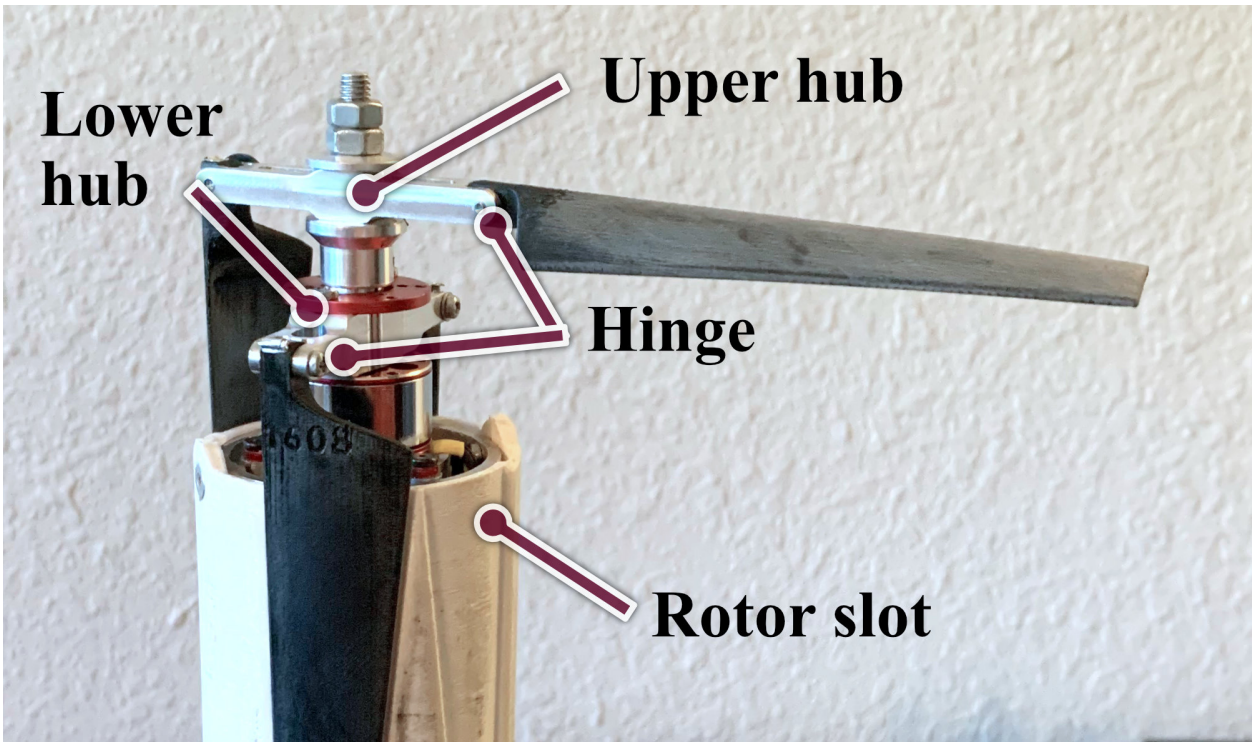

Figure 4.3: The rotor blades fold about a hinge and fit into a slot in the body.

4.3.1 Rotor Manufacturing

Given the specific design constraints on the rotors, a rapid prototyping technique was chosen for manufacturing. The rotors were printed on a Prusa I3 Mk3 [30] using Hatchbox®Polylactic Acid (PLA) with a layer height of 0.1 mm (0.004 in) with a 0.4 mm (0.016 in) nozzle. The low layer height was used to create a smooth surface finish, but the rotors still required post-processing. Unfortunately, the rotor blades thickness had to be set to 1.25 mm (0.049 in) due to limitation of the printer and filament. In the future, rotor blades manufactured from carbon fiber could be made

Table 4.1: Rotor parameters.

Parameter	Value
Radius	114.3 mm (4.5 in)
Thickness	1.25 mm (0.05 in)
N_o of blades	2
75% Chord	15 mm (0.59 in)
75% Pitch angle	17 deg
Twist	-12 deg
Taper ratio (root:tip)	2.2
Solidity	0.084

thinner to increase the overall rotor efficiency.

After printing, The rotor blades had to be post-processed to maximize rotor efficiency for the given blade geometry. The rotor blades were progressively sanded using 100, 180, and 320 grit sandpapers to smooth layer lines. The leading and trailing edges of the blades were also sanded and sharpened to improve the overall aerodynamic performance [7].

After post-processing, each individual blade was weighed and the blades were paired based on the mass. This was done to statically balance the rotor hub assemblies to reduce vibrations. The paired blades were then mounted to the upper and lower rotor hubs and placed on a rotor balance. When the assembly tended to rotate in favor of one side, steel washers were added to the screws securing the blades on the opposing side. This process was repeated until the system achieved balance, and the rotors were ready to be mounted on the vehicle or a test stand.

4.4 Propulsion System Testing

4.4.1 Rotor Testing Methods

A custom-designed hover test stand was used to quantify the performance of the rotors and to ensure that the printed rotors could withstand the loads at high rotational speeds. The hover stand, shown in Fig. 4.4, consists of a dual axis load cell to measure rotor thrust and torque, an optical rpm sensor,power supply and a data acquisitions (DAQ) unit. The coaxial motor unit was connected to a set of two electronic speed controllers (ESCs) so that the angular speeds of the

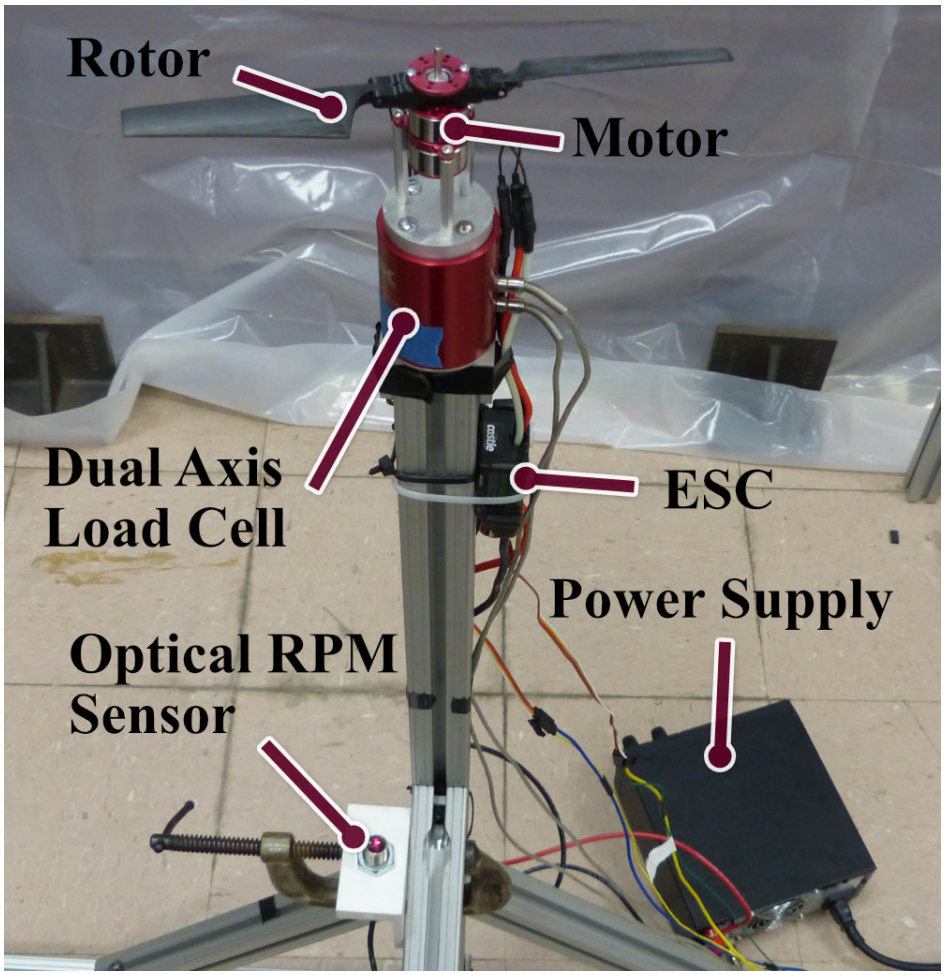

Figure 4.4: Hover test stand.

motor could be controlled independently. The power supply was set to 12 volts according to the motor manufacturers maximum recommended voltage of a 3-cell voltage.

The test data from the dual axis load cell and optical rpm sensor was recorded by a DAQ connected to a computer running a LabView program. Parameters that were measured included rotor thrust, torque and rpm were recorded to a file for post-processing. The rotor thrust and a torque were sampled at a rate of 1000 Hz, and each measurement was averaged over five seconds. The rpm readings were sampled at a rate of 100 Hz and also averaged over the same five second period.

The initial tests were conducted using a single rotor mounted to the upper motor of the coaxial

motor unit. A strip of reflective tape was placed on underside of the rotor for the optical sensor to detect. The rotor performance was measured at 10 different angular velocities corresponding to the motor-rotor response to 10 different PWM commands, and each data point was repeated five times. For each measurement, the rotor was brought to a rotational speed, and the data collection began once the the thrust and torque measurements reached steady state. Between each measurement, the rotor was stopped and the thrust and torque reading were tared to reduced sensor drift, but the procedure proved unnecessary due to minimal drift.

Similarly, the same procedure was followed when simultaneously testing both rotor mounted to the coaxial motor unit. For the coaxial motor experiments, only the lower rotor angular velocity could be measured due to the lack of a second optical sensors. The same PWM signal was sent to motors, which should correspond to approximately the same rotation speed for both rotors. Additionally, since both rotor were attached to the same load cell, only the combined thrust and torque could be measured.

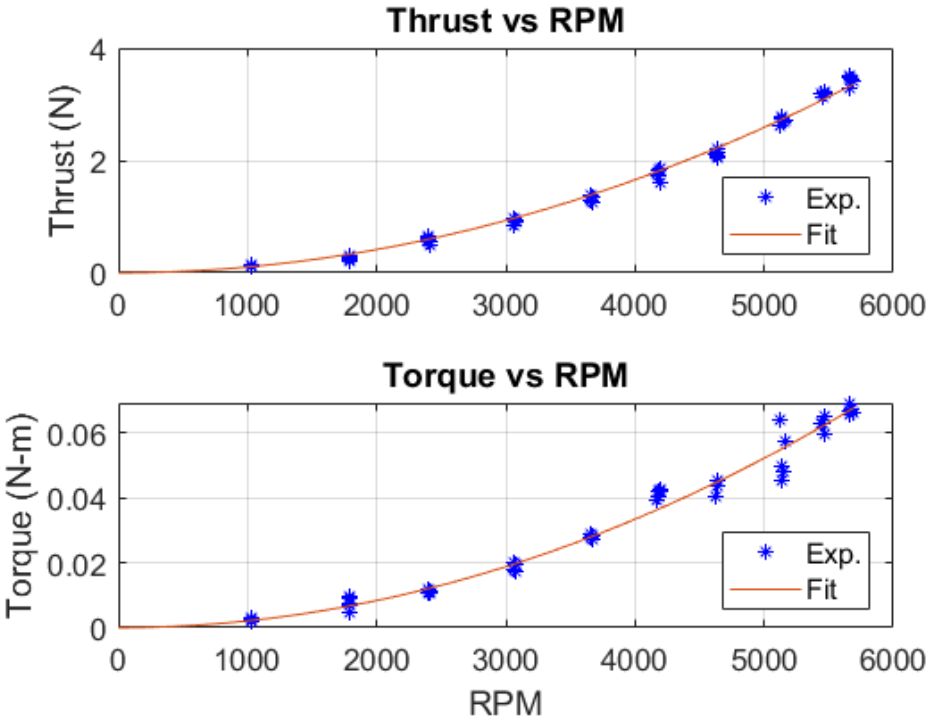

Figure 4.5: Single rotor: Thrust and torque vs. RPM.

4.4.2 Propulsion Test Results

The single rotor performance was used to determine the viability of the rotor design in terms of structural stiffness and overall performance. The resulting thrust and torque measurements for a single rotor are shown in Fig. 4.5. The mechanical power from the test is shown in Fig. 4.6. The test also verified that the rotor could withstand the rotating loads.

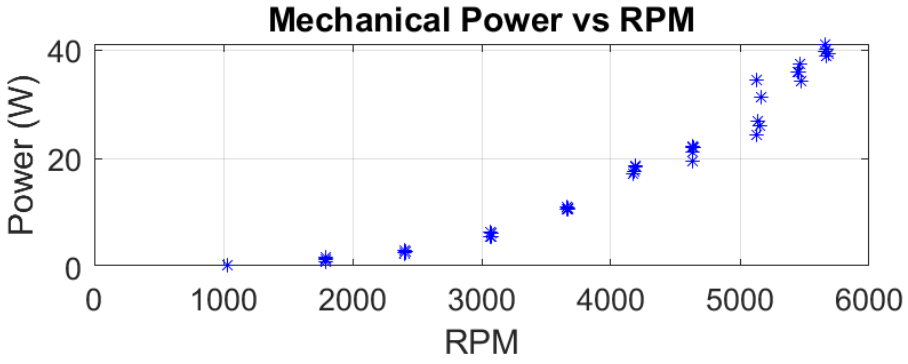

Figure 4.6: Single rotor: Mechanical power vs. RPM.

In addition to the single rotor measurement shown in Fig. 4.5, curve-fits were added to both thrust and torque measurement. The experimental data is plotted in blue and the curves are shown in red. Both quantities can be considered approximately quadratic with the rotation speed of the rotor. A quadratic least-squares regression was used to model the variation in both thrust and torque with respect to rotational velocity. The model for the single rotor thrust was given by the expression $T[N] = 1.035E{-}7 * rpm^2$, which resulted in a R^2 value of 0.994. For torque, the expression was $Q[Nm] = 2.090E{-}9 * rpm^2$, which resulted in a R^2 value of 0.981. Given that both of the R^2 values were above 0.9, this demonstrated that the models agreed well with the experimental data.

Next, the second rotor was added to the setup to measure the performance of the complete coaxial system. For the coaxial test, the rotors were tested at the same rpm, but the measured torque was approximately balanced as seen in Fig. 4.7 along with the resulting thrust. The coaxial

rotor test showed the rotor design exceeded the thrust requirement of 366 grams (3.59 N) for hover. It was noted that the net torque produced by the rotors was near zero. This result indicated that only minor adjustments may be necessary to trim the moment about the yawing axis of the vehicle during flight.

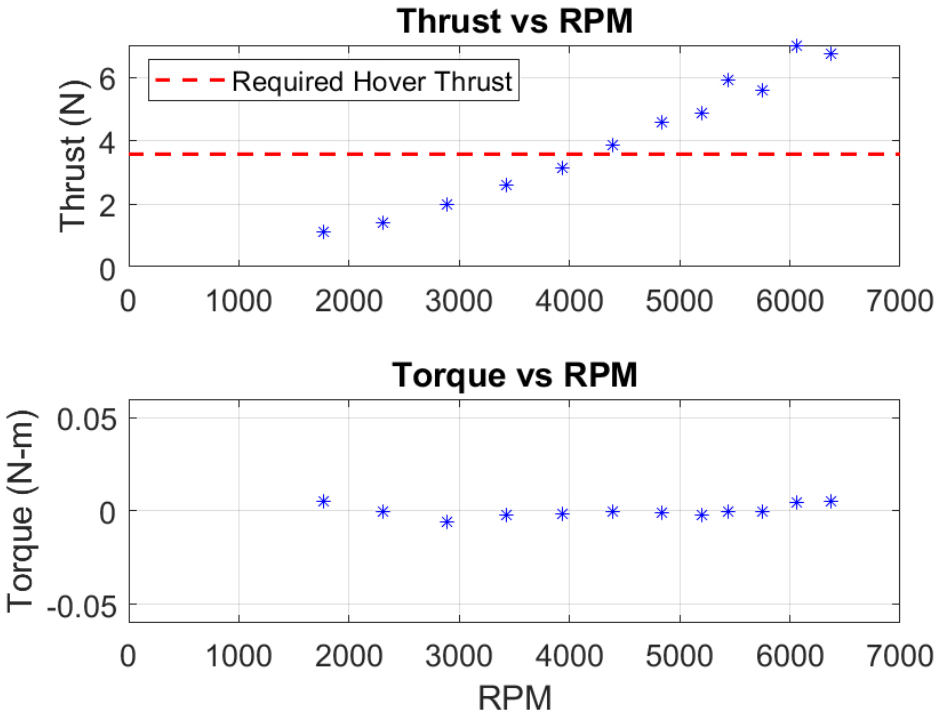

Figure 4.7: Coaxial rotor: Thrust and torque vs RPM.

4.4.3 Nondenominational Analysis

Once the rotor performance was measured, the nondimensional performance of the rotor could be characterized. Rotor performance is often described using nondimensional quantities such as coefficient of thrust (C_T), coefficient of torque (C_Q), and figure of merit (FM) [31]. The coefficient of thrust is given by the expression $C_T = T/\rho A(\Omega R)^2$, where T is the rotor thrust, ρ is the air density, A is the rotor disk area, Ω is the rotational speed of the rotor, and R is the rotor radius. The coefficient of torque is given by the expression $C_Q = Q/\rho A\Omega^2 R^3$, where Q is the aerodynamic

torque produced by the rotor, and the rest of the variables are the same as C_T. The figure of merit for a rotor is the ratio of ideal power to actual power aerodynamic needed to spin a rotor and is given by the expression $FM = C_T^{3/2}/\sqrt{2}C_Q$. Figure of merit is typically used as a measure of rotor aerodynamics efficiency, and the value ranges between 0 and 1.

Using the previous thrust and torque measurements for the single rotor experiments, the values of C_T and C_Q were calculated across the operating range of the rotor-motor combination. The results are show in Fig. 4.8 with the experimental data plotted in blue and the curve-fits in red using the previously discussed models for thrust and torque. In both instances of C_T and C_Q, both values are approximately constant across the measured range as expected since both quantities should primarily be functions of Ω^2 for a given rotor and air density. The calculated values of C_T and C_Q using the curve-fit data are $1.47E{-}2$ and $2.59E{-}3$, respectively.

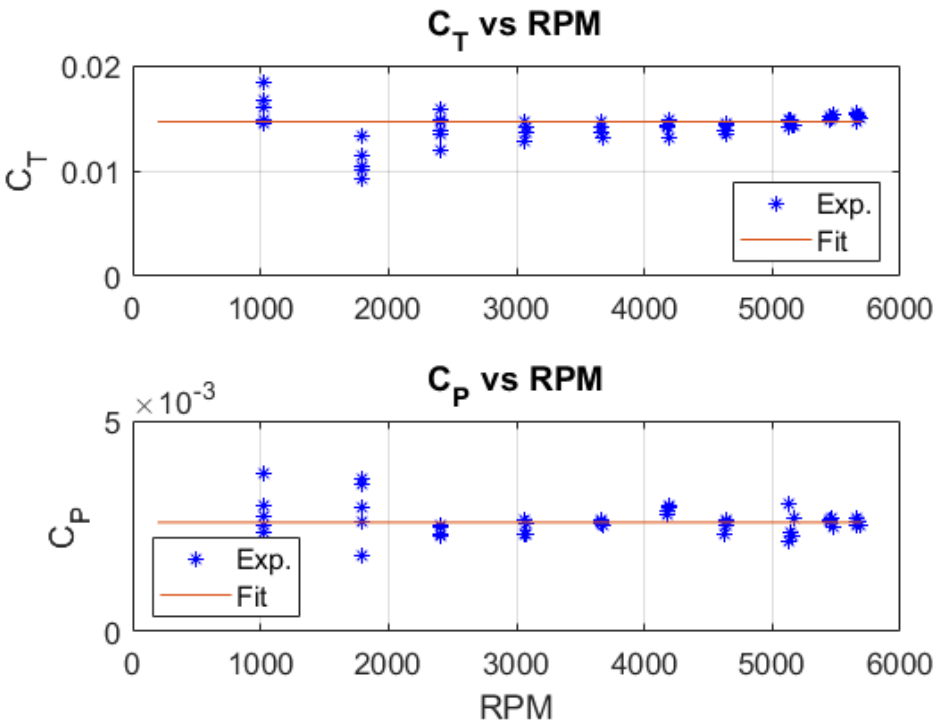

Figure 4.8: Single rotor: Coefficient of thrust (C_T) and torque (C_Q) vs. RPM.

The figure of merit was calculated using C_T and C_Q previously calculated from the single rotor measurements. A plot of figure of merit vs rpm is shown in Fig. 4.9 with experimental results plotted in blue and the curve-fit results in red. The calculated figure of merit using the curve-fit data was 0.487. In previous studies, an optimal figure of merit for a MAV-scale rotor has be show up to be as high as 0.65 [7, 29]. The relatively low figure of merit calculated for the current rotor design indicates that the design could be further optimized.

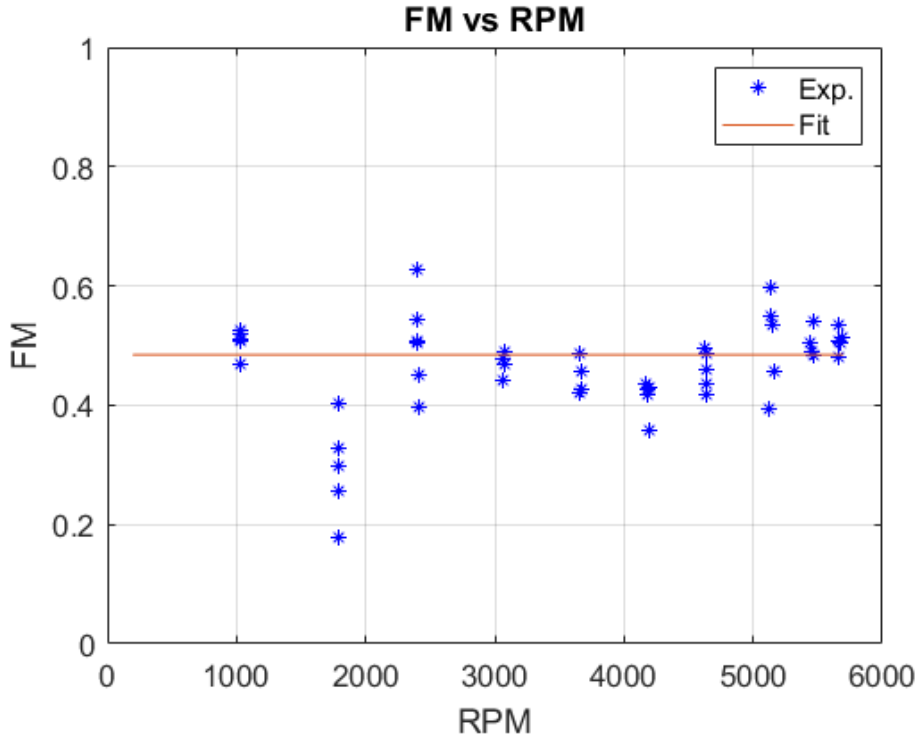

Figure 4.9: Single rotor: Figure of merit vs. RPM.

4.5 Concluding Remarks

This chapter discussed the coaxial motor unit used to greatly simplify the pitch and roll control mechanism and the rotor system used to propel the vehicle. The rotor design was driven by largely by the blade folding constraint, but some of the rotor parameter were derived from previous MAV rotor optimizations studies. The single and coaxial rotor experiments showed that the printed rotor

could withstand the aerodynamic loads and produce sufficient thrust for the vehicle. Further studies need to be conducted to measure and improve the combined motor-rotor efficiency to increase vehicle endurance. Higher rotor efficiency could be achieved by manufacturing thinner rotor blades and fine tuning other rotor parameters.

5. VEHICLE AVIONIC SYSTEMS AND FLIGHT CONTROLS

5.1 Avionics Hardware

The avionics system consists of an autopilot, telemetry module, serial receiver, and transmitter. The autopilot was selected for its small footprint and the ability to be customized for various vehicle platforms. The autopilot is responsible for processing sensor information and handling the flight control system. The flight test data is sent from the flight controller to a ground station via a wireless telemetry module.

5.1.1 Autopilot

Due to the size constraints, the vehicle required a custom and re-configurable autopilot for carrying out stabilization and control tasks. Hence a custom-designed ELKA-R autopilot was used because of its compact size (one inch square), lightweight (1.7 grams) and the ability to customize the flight control algorithm [2]. The autopilot is powered by a 5V regulator connected to the flight battery. A size comparison of the autopilot is shown in Fig. 5.1. ELKA-R is equipped with a STM32F405 microprocessor for all onboard computations tasks. The integrated MPU9250 is equipped with tri-axial accelerometers, gyroscope and magnetometer. These sensor measurements are used to determine the attitude of the vehicle. The details of the control system are included in the next section. Board supports up to 12 Pulse Width Modulation (PWM) actuators when two of the three Universal Asynchronous Receiver/Transmitter (UART) channels are converted to four PWM channels. The PWM channels are used to send control signals to the motors and actuators at a speed of up to 1000 Hz. The three UART channels can be used to read sensors or send data to other devices such as the telemetry module and PPM receiver.

5.1.2 Telemetry Module

The telemetry module is a XBee 3 Pro Zigbee 3.0 that operates at 2.4 GHz and is connected to the autopilot using a breakout board. This module allow ELKA-R to transmit data such as attitude and gyroscope measurements to a second XBee connected a ground station. The module is also

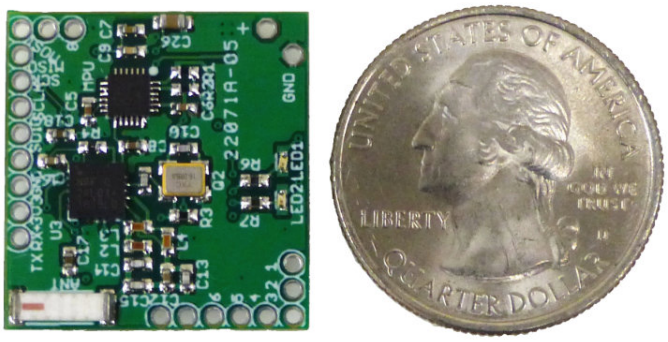

Figure 5.1: Compact 1.7g ELKA-R autopilot [2].

used to receive information from the ground station such as updated controller parameters and actuator trim values.

5.1.3 Transmitter and Receiver

The pilot's inputs are routed from the transmitter to the receiver, which is directly connected to the autopilot. A Taranis x9d transmitter is used to relay pilot commands, and it is capable of sending up to nine different control inputs at the same time. These inputs are encoded and sent to a FrSky R-XSR PPM receiver capable of reading eight different inputs signals to be sent to the autopilot. The autopilot processes the pilot commands and sends signals to the appropriate actuators.

5.2 Avionics Integration

This section discusses the interactions between the various components within the vehicle's avionics system that allows for flight stability and flight data collection. The major components include the autopilot for attitude stabilization, the motor and servos for initiating attitude changes, the ground station for telemetry and updating controller parameters, and the receiver for relaying pilot commands.

5.2.1 Control Mechanism

The control PWM signals sent by the autopilot to the servos and motors enable full control of the vehicle's states. As explained before, the thrust vectoring mechanism is actuated by two independent servos. The servos possess enough range to tilt the gimbal by ± 30 degrees in both the pitch and roll directions. This tilting creates a control moment about the CG causing the vehicle to rotate in the desired direction as shown in Fig. 5.2. To translate, the gimbal is first tilted in a desired direction until the body rotates, and then the vehicle reacts by translating in that direction.

The altitude and heading angle of the vehicle is controlled by varying the rpm of the two motors. To increase the altitude of the vehicle, the rpm of both the rotors needs to be simultaneously increased while maintaining the yaw torque balance. Since the upper rotor tends to aerodynamically interfere with the lower rotor, simply increasing the power to both motors would result in an imbalanced torque about the yaw axis as shown in Fig. 5.3. This torque is balanced by increasing power to the lower rotor and decreasing power to the upper rotor. The response is regulated according to the rate based feedback. The imbalance in the rotor torque is also used to yaw the vehicle during flight.

5.2.2 Ground Station and Receiver

The ground station consists of a computer with a Labview VI and a XBee module to send and receive telemetry from another XBee directly connected to the autopilot. The Labview program allows the operator to wirelessly update the feedback gains, change the trim points of the vehicle's actuators, and record telemetry data from the autopilot. The telemetry data includes the angular rates, accelerations, attitude angles, and the control signals sent to the servos and motors.

The transmitter and receiver facilitates the interaction between the pilot and the autopilot. The transmitter takes the pilot pitch, roll, yaw and throttle commands and sends them to the autopilot via the receiver. A separate channel was used to arm and disarm the actuators, and this measure was used to the disable the actuator feedback while the vehicle was loaded into the pneumatic cannon. The commands are converted to PWM actuator outputs after being processed by the

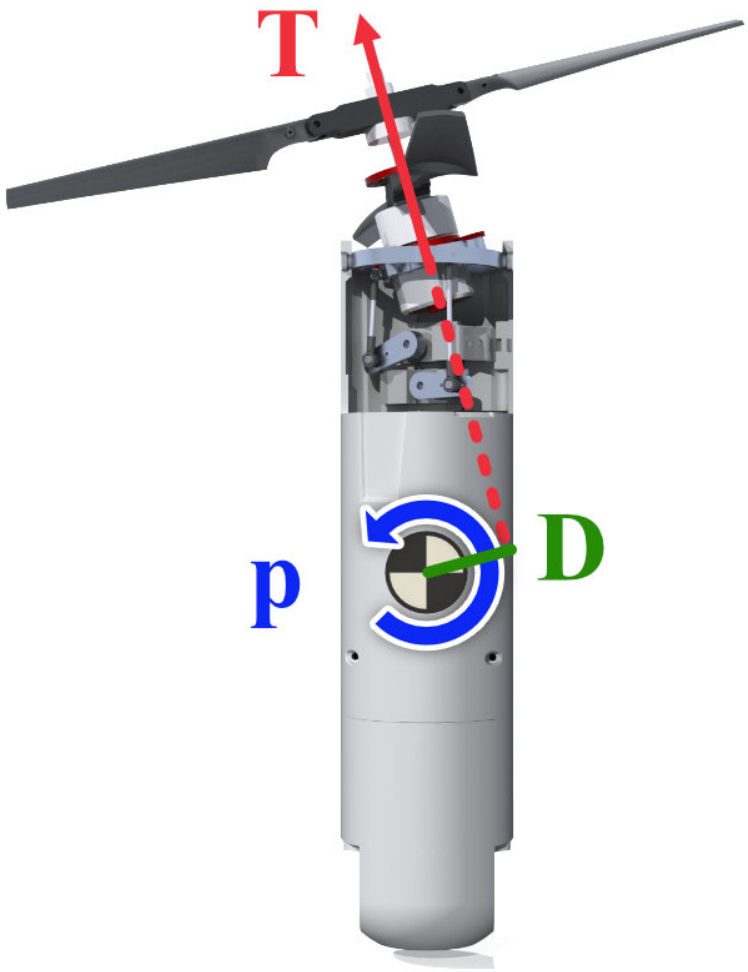

Figure 5.2: Rolling moment created by thrust-vectoring mechanism.

attitude feedback control programmed into the autopilot. The control scheme will be discussed in the following subsection.

5.2.3 Attitude Stabilization Overview

The attitude of the platform is obtained from the measured body-axis angular rates (gyroscope) and the tilt of the gravity vector (accelerometer). These measurements are filtered and fused to determine the pitch and roll attitude of the vehicle during flight. The Euler angles can be calculated

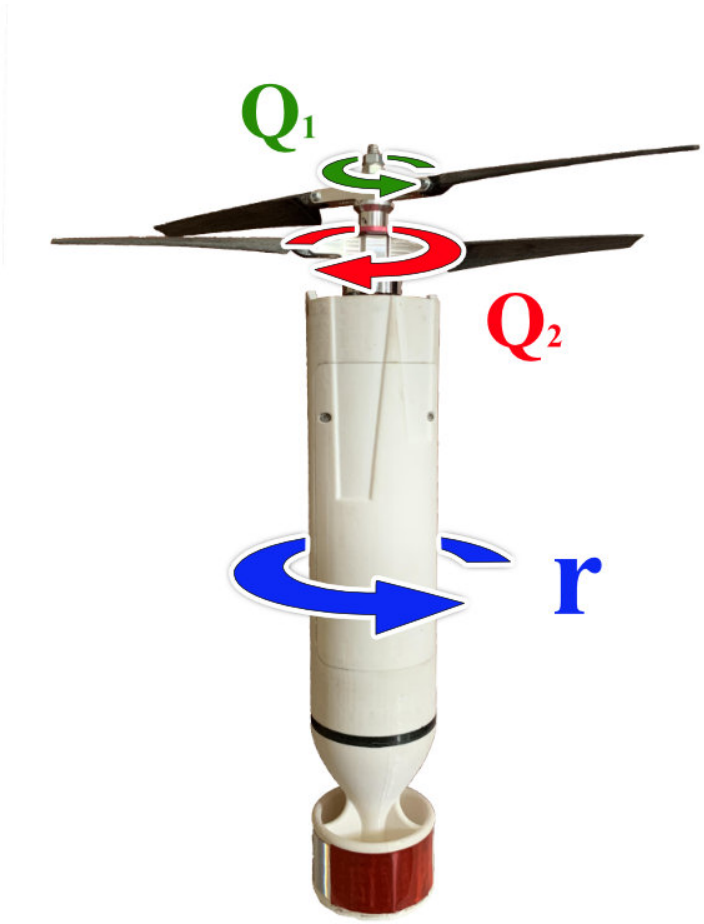

Figure 5.3: Yawing moment created by differentially varying the rpm of the motors.

by integrating the time history of the gyro measurements . However, gyro-based attitude measurement are known to drift over time [32]. The accelerometers are used to offer a stable bias for this drift, but the measurements are often polluted by high frequency noise [33]. Therefore, a complementary filter was implemented to calculate the roll and pitch Euler angles using a high-pass filter on the gyros data (4 Hz cut-off) and a low-pass filter for accelerometer data (6 Hz cut-off). These attitude measurements are fed back to the controller to stabilize the pitch, roll, and yaw of the vehicle.

In a previous study [23], the vehicle was stabilized using a proportional-derivative (PD) feedback controller, but the controller was then updated to a cascaded loop structure. The current

feedback structures will be discussed in the following subsection. In either case, the controller outputs a corrective signal from the feedback controller to the two motors and servos. The pitch and roll of vehicle is controlled by the servos through tilting the two-axis gimbal to create control moments to restore the vehicle to the desired attitude. Yaw of the vehicle is controlled by differentially varying the rotational speeds of the upper and lower rotors.

5.2.4 Attitude Stabilization Structure

The attitude stabilization is accomplished using a cascaded feedback structure composed of a faster inner loop and a slower outer loop that tracks a desired setpoint. According to Schmidt, the cascade controller structure can create more robust controller design [34]. The following control structure is presented in Fig. 5.4.

Starting from the outer loop for pitch and roll control, the pilot commands a desired pitch and roll attitude using a RC transmitter. The pitch and roll sticks on the transmitter are mapped to produce the desired outputs between ± 25 degrees. From there, the error between the desired and estimated attitude is scaled by the outer-loop proportional gain to get a desired rate. The desired rate is then passed as the setpoint for the inner-loop. In the inner-loop, the error between the desired rate and the measured rate is passed to a proportional-integral-derivative (PID) feedback controller. The controller output is directly converted into servo commands for the thrust-vectoring mechanism that initiate the desired correction to the vehicle. The outer-loop runs at 1/5th the speed of the inner loop to prevent the outer-loop from overriding the inner-loop. This is important because the inner-loop is sampled at a higher frequency than the estimation of the attitude angles.

Yaw control is handled using a similar methodology as pitch/roll control, however, with the absence of the outer loop. Since heading hold has not been implemented on the vehicle, the pilot commands a desired yaw rate instead. The yaw stick on the transmitter is mapped between $\pm$ 250 degrees per second. As before, the desired rate is compared against the measure yaw rate and the difference is passed into a PID feedback controller. The output of the controller is a differential yaw command that is provided by increasing power to one rotor while reducing power to the other. Since the inertia of the yaw axis of the smaller than that of the pitch and roll axes, vibrations

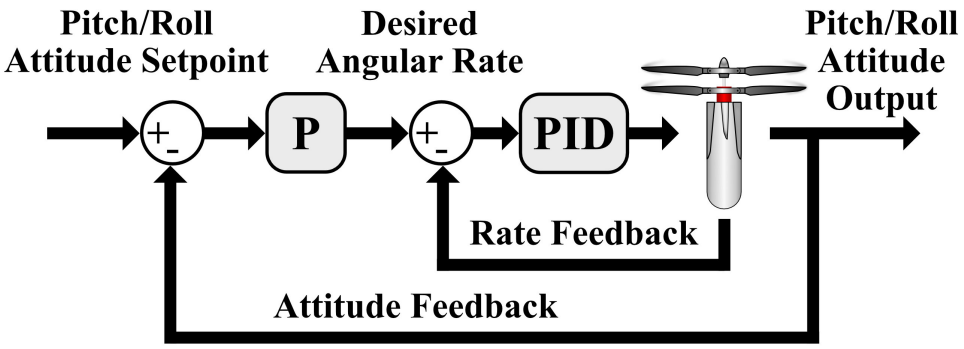

(a) Pitch and roll attitude feedback.

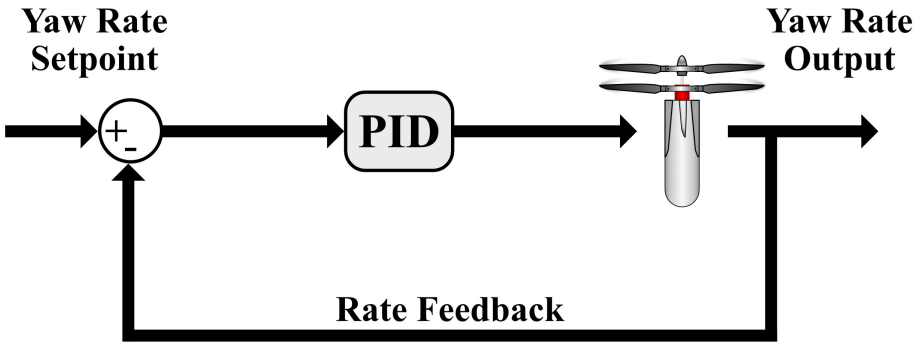

(b) Yaw rate feedback.

Figure 5.4: Controller feedback diagram.

generated from rotors tends to adversely affect the yaw feedback. However, the effect is mitigated by filtering the gyro measurements below the rotor operating frequencies and setting the derivative term of the controller to zero.

5.3 Rotor Start-up

Since the rotors needed to be folded to be inserted into the cannon for the vertical launch of the vehicle, an unfolding strategy needed to be perfected before the launch. The most obvious method was to spin up the upper rotor followed by the lower. This sequence would prevent the rotors from impacting each other on startup. The centrifugal force acting on the blades would allow the them to naturally unfold and deploy.

The rotor startup sequence was programmed into the autopilot and was triggered after the throttle signal passed a preset threshold. When the vehicle is powered, the servos hold the thrust-vectoring mechanism in the trim position with the feedback controller disabled while the vehicle is in the barrel of the cannon. In the trim position, the blades are retained within their respective slots in the fuselage. After launch, once throttle is above the threshold, the upper rotor begins to spin-up. Approximately a quarter of a second later, the lower rotor begins to spin. This short delay is long enough to keep the counter-rotating blades from impacting each other. Once both rotors are spinning, the autopilot begins relaying controller commands to stabilize the vehicle.

The startup sequence was tested numerous times on the vehicle before flight. As long as the friction in the flapping hinge is not too high, the rotors were shown to reliably spin up without any issues. A video of the rotor startup sequence can be found in Ref. 35, and a few frames from the video can be viewed in Fig. 5.5. The first frame show the instant before the upper rotor begins to spin. The second and third frames show snapshots in time of the upper and lower blades, respectively, as the rotors begin to unfold. In the last frame, the rotors appear fully deployed.

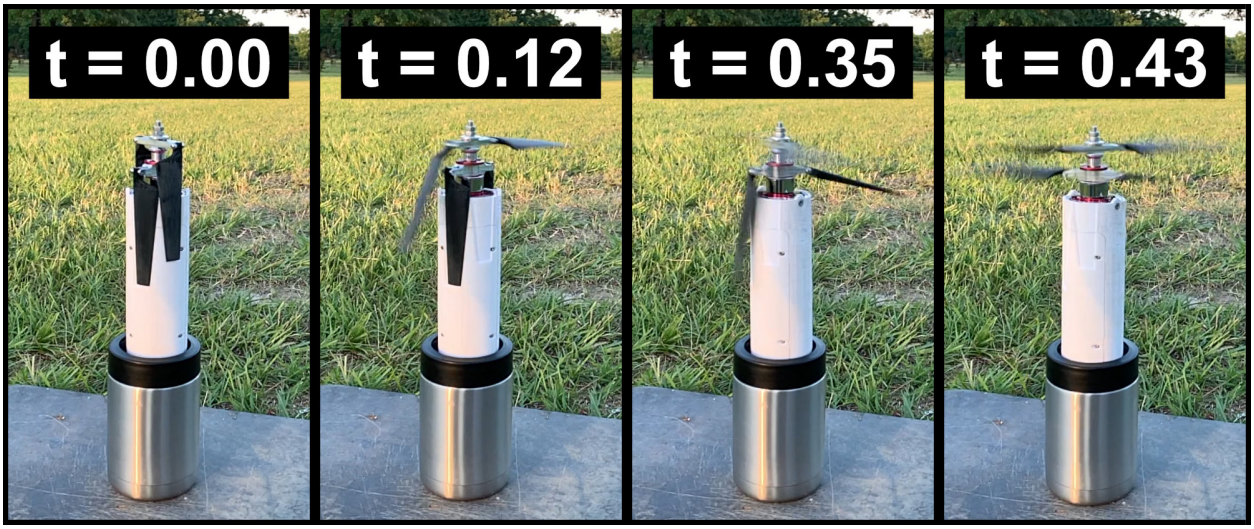

Figure 5.5: Rotor startup sequence.

6. FUSELAGE AND FIN DESIGN

6.1 Fuselage Design

The body of the vehicle acts as the anchor point for all of the major components and is designed to fit within the air cannon. The body also consists of a side panel and a battery cage to access the electronics and battery. The outer diameter of the body is 51.5 mm to fit within a standard two inch schedule 40 pipe used for the barrel of the pneumatic cannon. The thrust vectoring mechanism is attached to the main body using press nuts, which are inserted in the hole on the upper portion of the body, and shoulder screws inserted in the outer gimbal. Around outer gimbal are slots that were made to house the folded rotor blades. Below the gimbal are the mounts for the servos that are secured using self tapping screws through the servos into the mounts. The autopilot and the telemetry modules are mounted to a breakout board that serves as a mounting plate, which is connected to the main body using threaded inserts and vibration dampening screws. This assembly is shown in Fig. 6.1. The two ESCs are mounted to the inner wall of the fuselage underneath the autopilot, and the receiver is fixed to the top of the telemetry module with double-sided tape. There is an opening at the bottom of fuselage to receive the battery cage that served as a rigid mount to prevent the lithium polymer battery from shifting during flight. The cage also acts as an access point to easily allow the battery to be replaced while testing by removing the fin assembly. All of the internal components are accessible by the access panel that conforms to main body and is attached by four screws.

6.1.1 Fuselage Fabrication

The main body and access panel were rapid prototyped using ABS plastic to ensure a secure fit for all of the internal components. Plastic threaded insert were added to create mounting points for the gimbal, breakout board, and battery cage. The insert allowed the internal components to be removed without wearing down the holes in the plastic. This configuration is important for parts that are frequently removed from the fuselage such as the access panel. The outside of the main

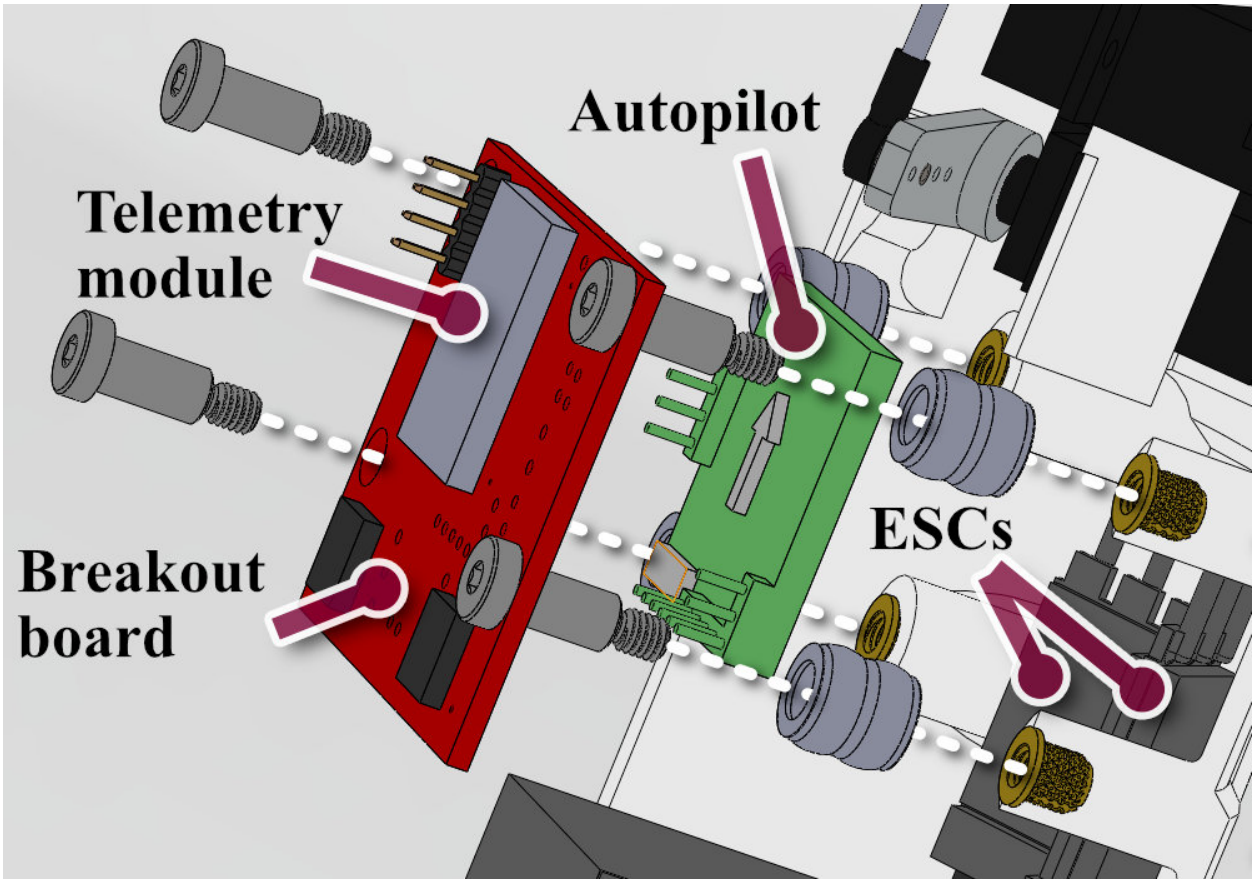

Figure 6.1: Exploded view of the autopilot and telemetry modules placement on the vehicle.

body and access panel were sanded to create smooth contact surface between the body and cannon barrel.

6.2 Fin Assembly

The fin assembly was designed to stabilize the the vehicle during the vertical launch phase. Similar to the fuselage, the fin was rapid prototyped using ABS plastic. The main purpose of the fin was to shift the aerodynamic center (AC) of the below the center of gravity (CG) to provide passive aerodynamic static stability during the projectile phase [34]. The fin assembly consists of three smaller fins connected to the body on the inside and a structural ring on the outside. An isometric view and bottom view of the fin assembly is show in Fig. 6.2. The fin design proved to be sufficient via tests conducted with the dummy to verify passive stability during the projectile

phase, and a video of one of the tests can be viewed in Ref. 36. The fin also serves as an access point to the battery.

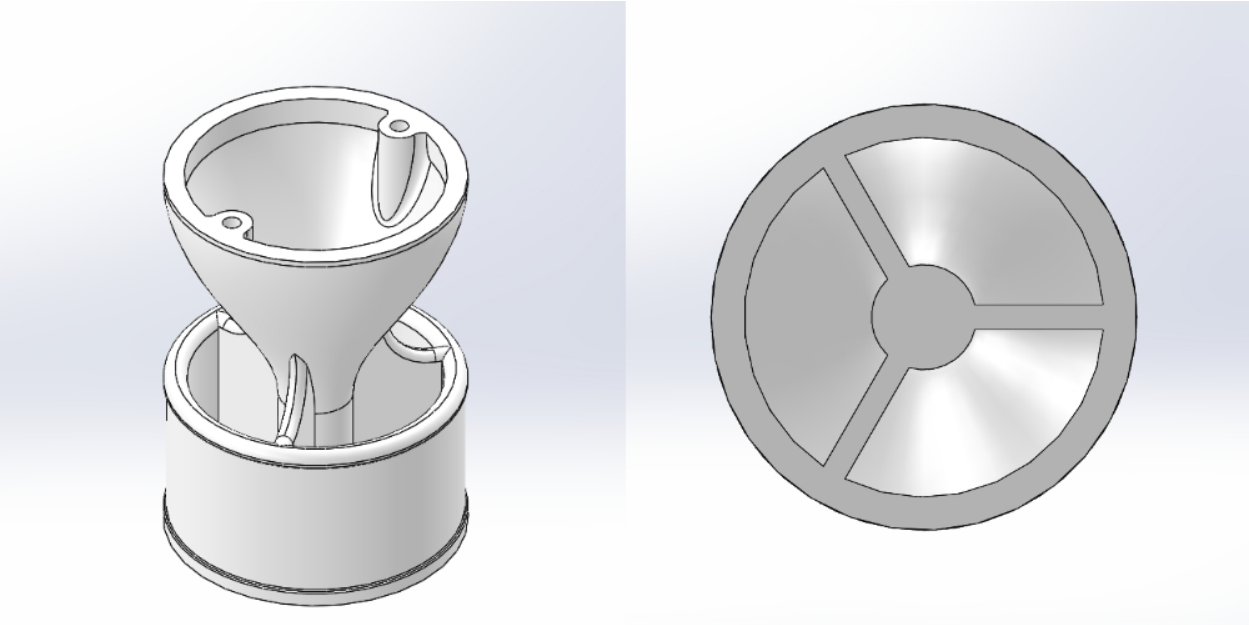

Figure 6.2: Isometric view (left) and bottom view (right) of the fin assembly.

7. WIND TUNNEL TESTING

7.1 Wind Tunnel Testing Overview

This section discusses the process used to verify the ability of the controller and the thrust-vectoring mechanism to handle the disturbances that may be experienced by the vehicle during recovery from launch or flight in gusty conditions. This process began by tuning the pitching response of the vehicle on a single degree-of-freedom (DOF) stand and then subjecting the vehicle to a disturbance in a wind tunnel. The results of these test provided enough confidence in the controller to begin free flight testing. The effectiveness of the swashplateless, thrust-vectoring mechanism was demonstrated.

7.2 Test Stand Description

A simple test stand for the vehicle was constructed to test the pitch response of the controller. The stand was composed of two vertical posts both connected to a base plate at the bottom, and a mounting hole for the pitching axes of the vehicle to pass though. The vehicle was mounted on the stand using a set of shoulder screws on the left and right sides of he vehicle. The shoulder screws were inserted though bearing placed in the mounting hole of the posts, and bolted into threaded inserts on the exterior of the vehicle. The threaded inserts on the vehicles were positioned such that the axis formed by the shoulder screw passed through the CG of the vehicle. The stand described here is shown in Fig. 7.1.

7.3 Disturbance Rejection Testing

Although the vehicle configuration for these tests does not reflect the vertical launch configuration, the tests provided valuable insights into the behavior of the controller and the thrust-vectoring mechanism. The ballistic configuration (projectile launched at an angle much lesser that 90 degrees) of the vehicle was used in these tests. The ability of the controller to reject gust disturbances was tested by placing the stand and the vehicle in a closed-circuit low-speed wind tunnel. The objective of this test was to demonstrate that the vehicle can hold a desired pitch forward attitude in

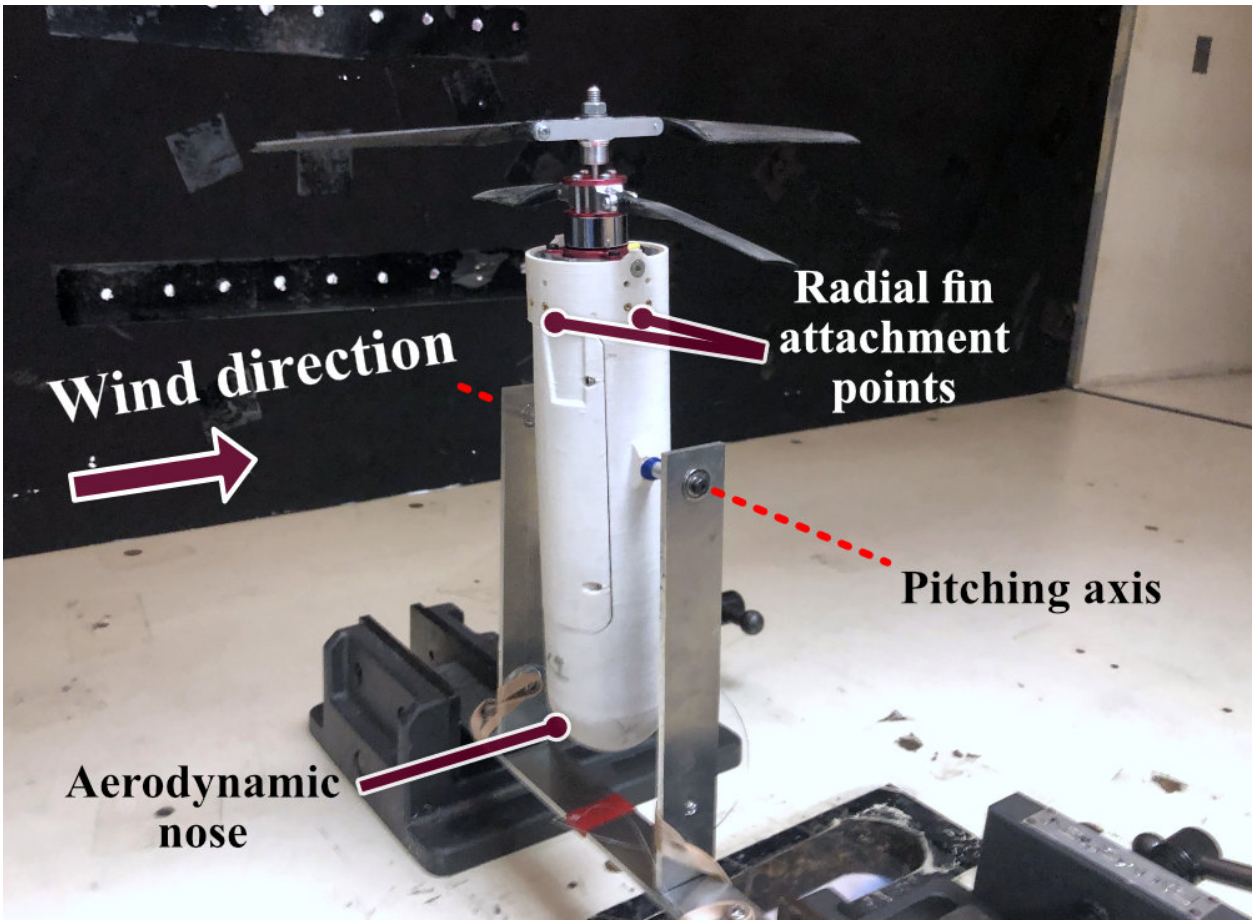

Figure 7.1: Single DOF stand in wind tunnel for forward flight testing.

the presence of a steady wind gust.

7.3.1 Methodology

For this test, the vehicle was placed in an upright position on the stand, and the stand was held by clamps in the center of the 3ft by 4ft wind tunnel test section (Fig. 7.1). Once the vehicle and ground station were powered, the test section was sealed. The connection between the vehicle and the ground station was initiated, and the desired controller gains and trims were updated before testing. The rotors on the vehicle were powered, the rotational speed was set to the hover rpm and the feedback attitude control was enabled. The airspeed of the wind tunnel was set to the desired value. Vehicle telemetry was set to begin recording the attitude response. Then a step input was provided to command the vehicle to a 25 degree pitch forward attitude. The command was held

for five seconds and then brought back to zero for five more seconds.

7.3.2 Results

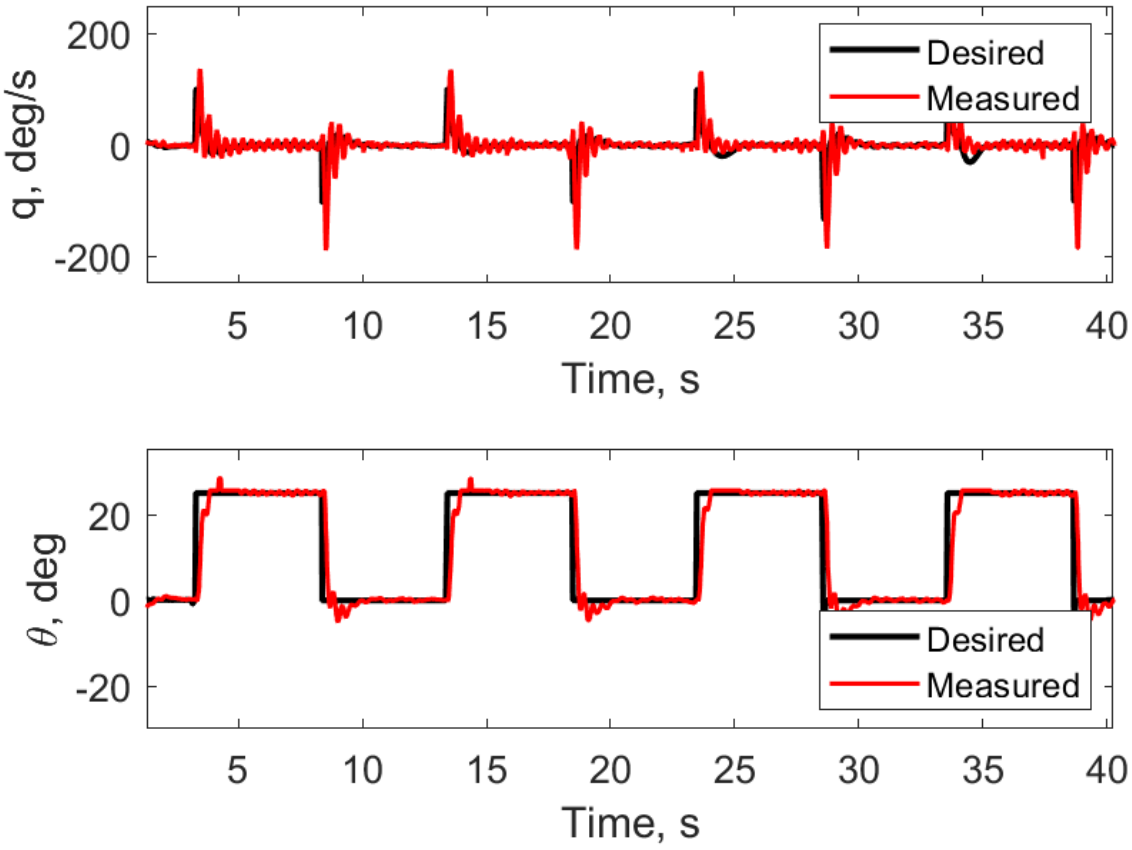

Figure 7.2: Pitch response to step input when the vehicle was subjected to a 5 m/s wind speed.

These tests were performed at wind speeds between 3 and 6 meters per second (m/s), and the pitch response was recorded using the telemetry module. A video of one of these tests can be viewed in Ref. 37, and the results are shown in Fig. 7.2. For this test, the vehicle was subjected to a 5 m/s wind speed, and the controller was able to track the commanded 25 degree step input. Similar performance was noted at 3 m/s; however, at 6 m/s, the vehicle took longer to reach the desired attitude. Although, after testing the vehicle in free flight, it was noted that in forward flight

and in the presence of a mild wind, the vehicle's attitude in pitch rarely exceeded 10 degrees. In hindsight, a 10 degree step input could have been a more representative case as opposed to 25 degrees.

7.4 Wind Tunnel Tests to Simulate Axial Descending Flight

In the next phase of testing, the vehicle was mounted horizontally on the stand so that wind direction was parallel with the vertical axis of the vehicle. This test was meant to replicate the axial flow conditions that will be experienced by the vehicle during the crucial descending plus transitioning phase of the trajectory. In this state, the rotors will be deployed and the vehicle will utilize the rotor thrust to brake or decelerate to a hovering state. During breaking, vortex ring state could be encountered, which could lead to loss of control due to highly unsteady rotor aerodynamics at certain descent speeds [31].

7.4.1 Methodology

Before the vehicle was tested in this configuration, weights were added to the lower portion of the vehicle to ensure that the CG passed though the pitching axis and vehicle remained horizontal. Similar to the previous test, stand was placed in the test section as shown in Fig. 7.3, and the vehicle and ground station were powered. Once the test section was sealed, the rotors were powered on to prevent windmilling before the wind tunnel was brought up to speed. This important step ensured that both rotors were producing thrust during the test because the ESCs tended to shutdown if the ESCs could not overcome the windmilling rotors. The vehicle was commanded to hold the horizontal attitude as the airspeed was increased to the desired value. The vehicle response was observed, and the telemetry data was recorded on the ground station.

7.4.2 Results

The first set of descent experiments were performed without fins to determine if fins were necessary for powered, controlled descent. If it was shown that fins were not necessary for the ballistic launch, the overall design could be simplified. For these tests, the wind speed was varied between 3 and 6 m/s and three different throttle settings. For the lowest throttle setting (results in lower

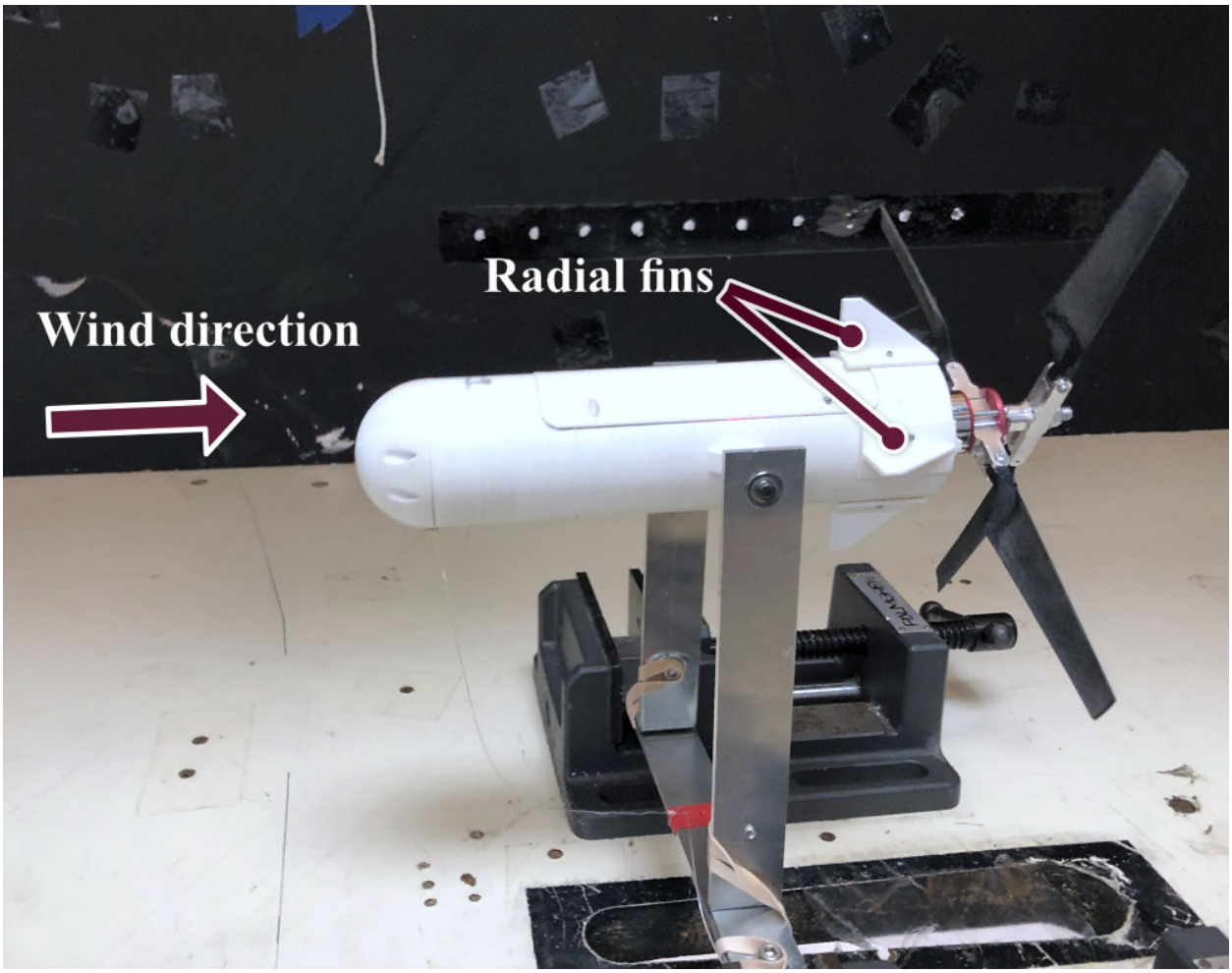

Figure 7.3: Single DOF stand in wind tunnel for axial descent testing.

deceleration), the controller could prevent the pitch attitude from deviating more than 20 degrees in either direction from the horizontal. At a medium throttle setting (moderate deceleration), the the controller met the same criteria until wind speed was increased beyond 5 m/s. The result for the 4 m/s case at a medium throttle setting is presented in Fig. 7.4. When the throttle was increased to the high setting (high deceleration), the controller was unable to stabilize the vehicle at any speeds. This instability could have due to the vehicle entering vortex ring state.

In the next set of experiments, the radial fins were added to determine if fins could expand the range of wind speeds for which the controller could stabilize the vehicle. The tests were performed at the medium throttle setting, and the wind speed was varied between 3 and 6 m/s as before. As

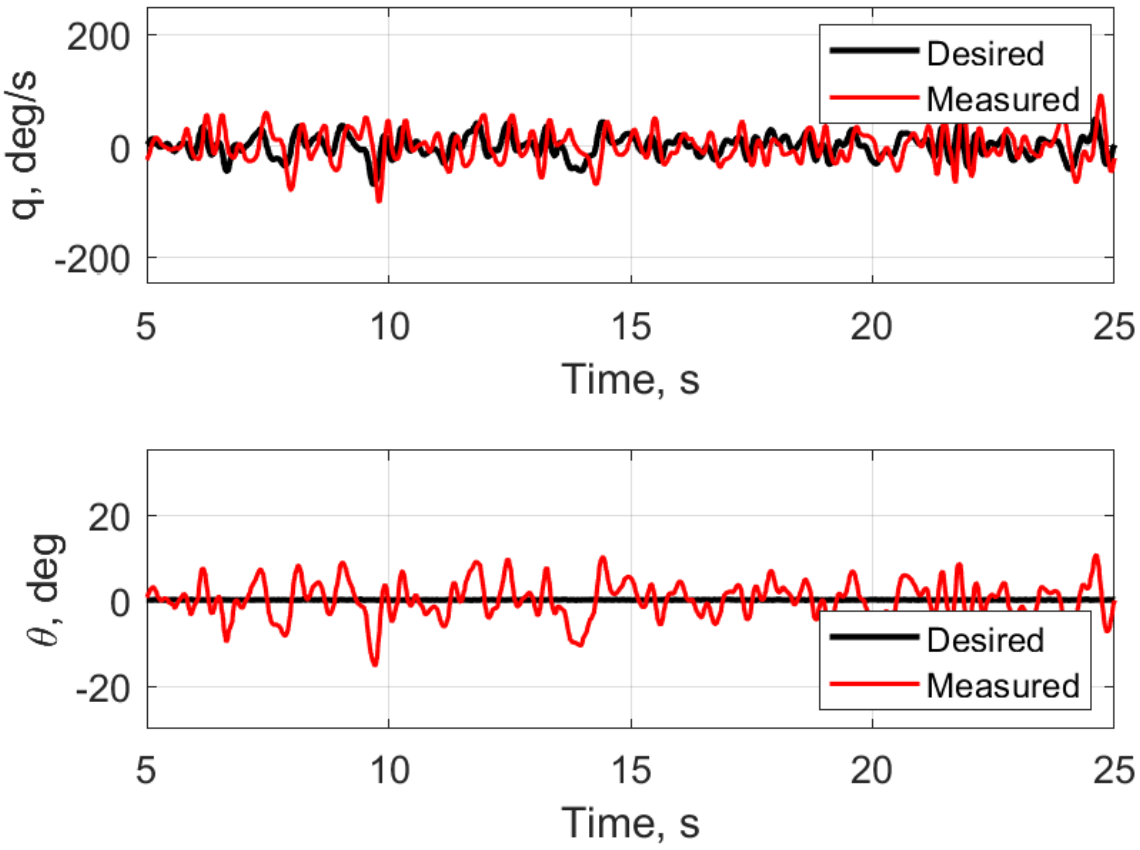

Figure 7.4: Pitch response to descending flight without fins when the vehicle was subjected to a 4 m/s wind speed.

expected, with the addition of fins, the stability of the system seemed to improve with increased wind speed. The same controller gains were used as the previous tests. The vehicle with fins remained stable for the full range of wind speeds tested. The pitch response of the vehicle at a wind speed of 6 m/s is plotted in Fig. 7.5.

7.5 Concluding Remarks

This chapter discussed the wind tunnel experiments to check the control authority of the vehicle in both forward flight can axial descent. The controller response was tuned for both flight conditions, and the effectiveness of the thrust-vectoring mechanism was shown. Although the controller could stabilize the vehicle without the fins, the wind tunnel testing demonstrated that the

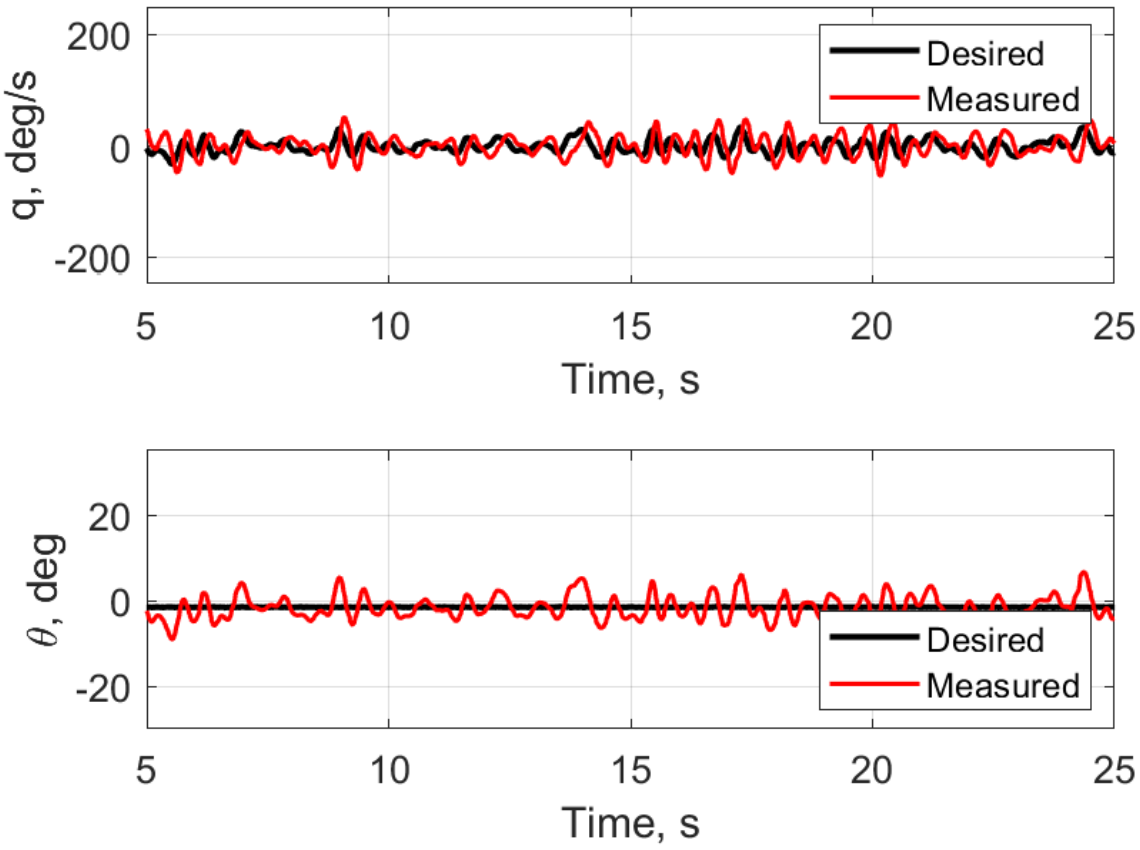

Figure 7.5: Pitch response to descending flight with fins when the vehicle was subjected to a 6 m/s wind speed.

flight envelope could be increased with fins. In the next phase of testing, in-flight drop tests were conducted to bring in the 6-DOF vehicle dynamics, which were not present in the wind tunnel tests. The results of the drop tests are presented in the next section.

8. HOVER AND FREE-FLIGHT TESTING

8.1 Flight Testing Overview

In the next stage of testing, the vehicle was removed from the test stand to begin free flight testing. Free flight testing was composed of basic hover testing and drop testing. Hover testing ensured that the vehicle was capable of stable flight under indoor and outdoor conditions. Drop testing were considered a continuation of descent testing performed in the wind tunnel on the stand. These tests served as a key milestone to complete a successful launch and recovery.

8.2 Hover Testing

8.2.1 Methodology

For indoor flight testing, the vehicle was flown in an 8x8x8ft enclosure which was constructed using aluminum 80-20 framing and wrapped with thin plastic sheets. The purpose of this enclosure is to minimize possible damage to the vehicle in the event of a hard landing or crash. The floor is also slightly elevated to reduce the impact on the vehicle in the event of a hard landing. When testing, the vehicle takes off from a platform that holds the vehicle upright to prevent the vehicle from tipping over during takeoff. The streamlined nose-cone located on the bottom of the vehicle creates difficulties when landing; therefore the vehicle is often grabbed by the pilot mid-flight as opposed to landing. This reduces the risk of damaging the rotors or the servos.

8.2.2 Flight Testing Results

The first set of hover tests were performed to verify that the controller gains that resulted from stand testing were transferable to free flight conditions. Since the vehicle is approximately axi-symmetric about the yaw axis, the controller pitch gains determined from stand testing were also applied to the roll gains. The yaw gains were tuned via flight testing. The vehicle was flown with the previously determined gains, but fine tuning was necessary to improve the vehicle response in hovering flight. The pitch response shown in Fig. 8.1 indicated that the controller is able to hold

zero rates and attitude angles, and this result was similar in the case of roll response as well.

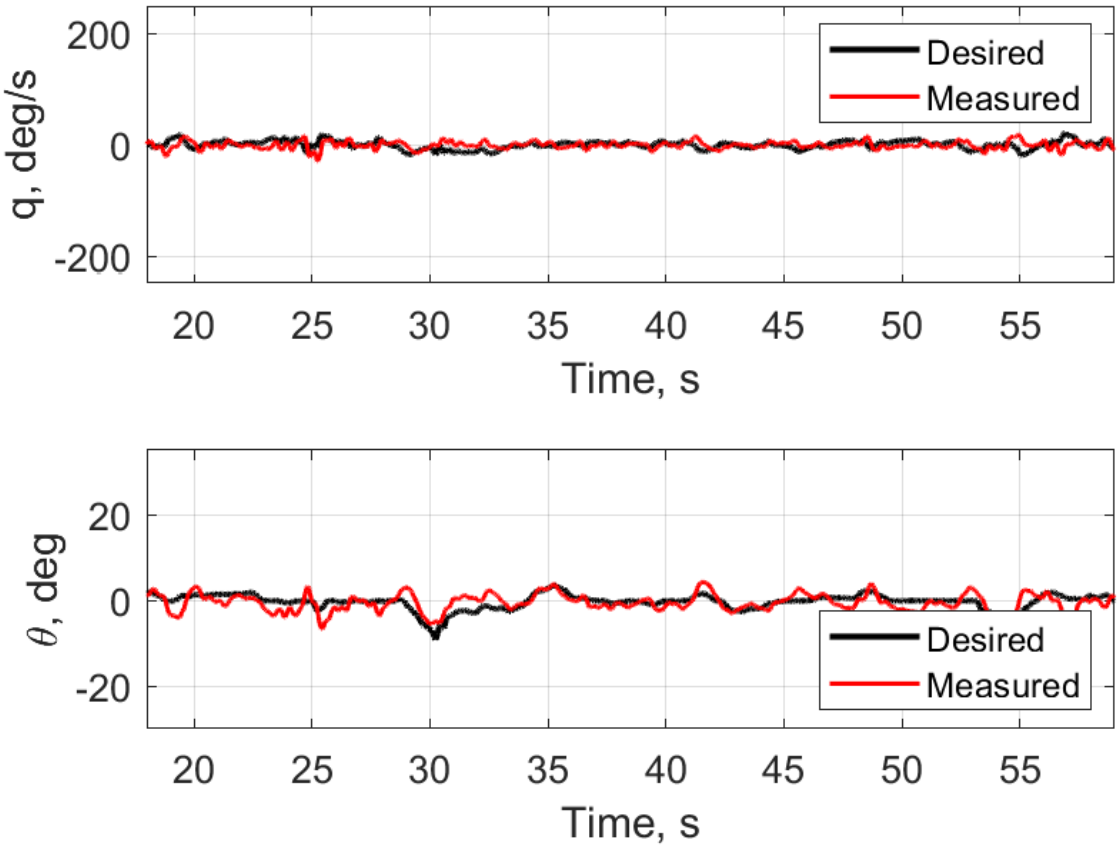

Figure 8.1: Pitch response during hover.

8.3 In-Flight Drop Testing

In-flight drop tests were attempted to replicate the transition from the descent phase of the flight to stable hovering without actually launching the vehicle from the pneumatic cannon. The purpose of the test was verify that the controller could stabilized the vehicle during descent.

8.3.1 Methodology

The descent phase of flight was mimicked by flying the vehicle up to an altitude of 40 feet above ground and then reducing the thrust to allow the vehicle to drop vertically to reach high descent

rates. After falling for almost one second, the thrust was increased above the value required for hover to decelerate the vehicle to a hovering state. The ground station recorded the response of the vehicle, and a video of the test can been viewed in Ref. 38.

8.3.2 In-Flight Drop Testing Results

The vehicle was flown inside a hanger with 40 foot ceilings without the fin to determine if the vehicle could recover. As described previously, the vehicle was flown to a high altitude and the throttle was reduced. With the cascaded controller, the vehicle entered a low amplitude oscillatory mode in pitch and roll but, it recovered successfully. The test was repeated several times during the flight. The plot in Fig. 8.2 shows the pitch response as the throttle (show in blue) is briefly reduced and then increased.

8.4 Flight Testing Conclusions

This chapter discussed the free flight experiment perform with vehicle after feedback controller was tuned in the wind tunnel. The vehicle was first flown indoor in the absence of disturbances to verify that the controller was tuned and could hold a horizontal attitude. Next, the axial descent tests were repeated with the vehicle in free flight to determine the ability of the controller to stabilize the vehicle in that adverse condition. Despite the presence of a low amplitude oscillation which appears as the throttle was increased, the feedback controller maintained stable flight.

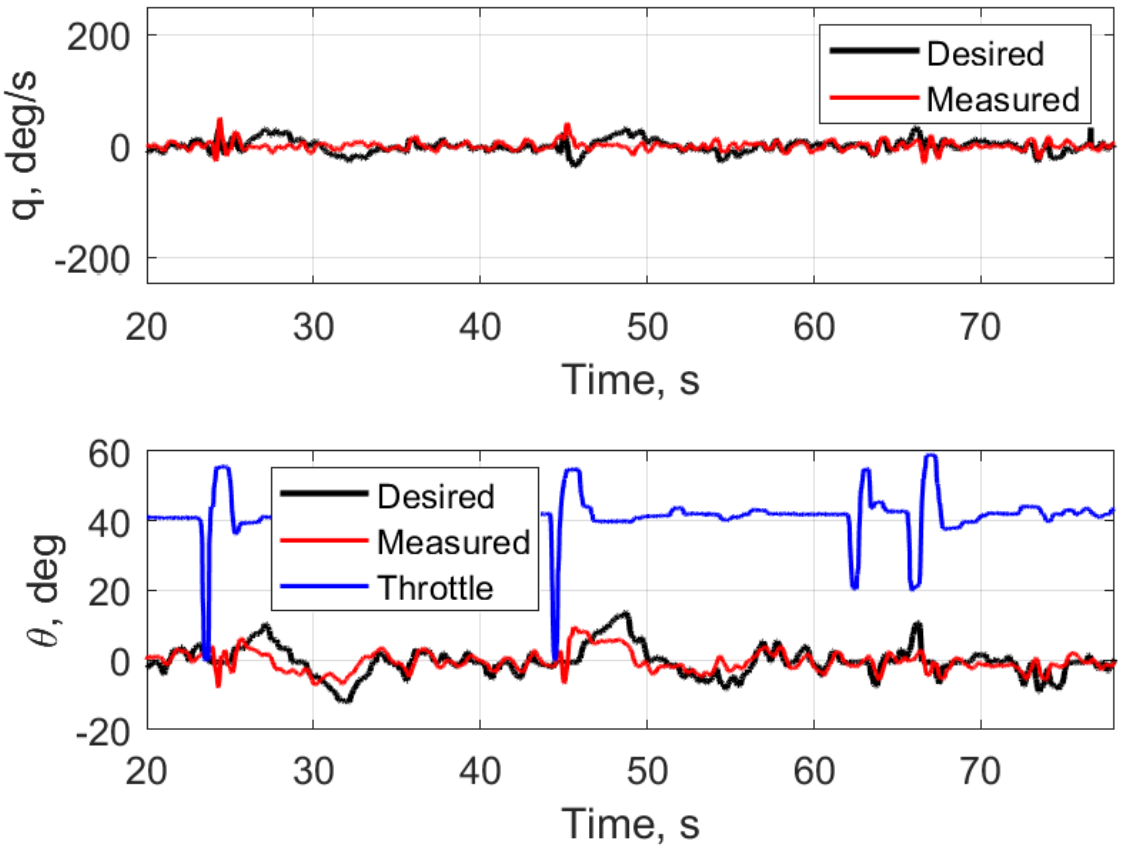

Figure 8.2: Pitch response during the drop test.

9. VERTICAL LAUNCH TESTING

9.1 Vertical Launch Testing Overview

This section discuses the final steps taken before the vehicle could be launched in the vertical configuration. A "dummy" with similar shape and inertial properties as the actual vehicle was launched vertically from a pneumatic cannon to check if the fin assembly could stabilize the vehicle after launch. Before the vehicle could be launched, the rotor startup sequence (deployment from the folded state) had to be tested. Finally, a vertical launch of the vehicle was performed.

9.2 Vertical Dummy Launch Testing

The analogue to the flying vehicle or a “dummy” was designed to test the passive stability of the vehicle with the fin assembly during the unpowered projectile phase of flight. The dummy could be launched without risking the more fragile components in the actual flying vehicle. More importantly, the dummy launch serves as a perfect rehearsal for the vehicle launch. The dummy was designed as close as possible to the actual flying vehicle and consisted of all the same components except for the actuators, thrust-vectoring mechanism, and flight battery. Similar shape, overall dimensions, and mass distribution were used to ensure that the dynamics of the dummy during the vertical launch would be close to that of the flying platform.

The dummy was also used to test the response of the autopilot’s sensors after experiencing the high initial launch acceleration to make sure their ratings are not exceeded. Since both accelerometer and the gyro measurements are used to estimate the vehicle attitude for stabilization, it was crucial to the verify that sensors would be reliable after the launch phase.

9.2.1 Methodology

The test launch of the dummy was performed in an open and relatively flat field that was free of obstacles and people. First, the pneumatic cannon was pressured to 70 psi (482 kPa), and then the cannon was positioned at a near vertical angle. The cannon can be viewed in Fig. 9.1. The dummy was placed on a level surface, and then the battery was plugged in to power the electronics. Once

the ground station began receiving from the telemetry module, the dummy was lowered into the cannon with the fin assembly pointing down.The relative locations of the AC and CG was designed to prevent the dummy from tumbling during launch. Finally, the ground station began recording data, and the solenoid controlled valve was triggered to launch the dummy.

Figure 9.1: The custom pneumatic cannon used for vertical launch experiments.

9.2.2 Vertical Dummy Launch Results

Overall, the launch of the dummy appeared to be stable from launch until the apex of the trajectory was reached. After reaching the apex, as expected, the dummy began to tumble at low speeds, and the response is shown in Fig. 9.2. According the the vertical accelerometer readings (blue line), the launch occurred at 14.5 seconds and the dummy impacted the ground at 18.7 seconds. If it is assumed that the apex is reached at half of the flight time, the dummy remained at an attitude less than $\pm$ 45 degree before that point. This test demonstrated that the fin assembly could stabilize the dummy during the first half of the flight, and the test also proved that the sensor measurements are reliable after the launch.

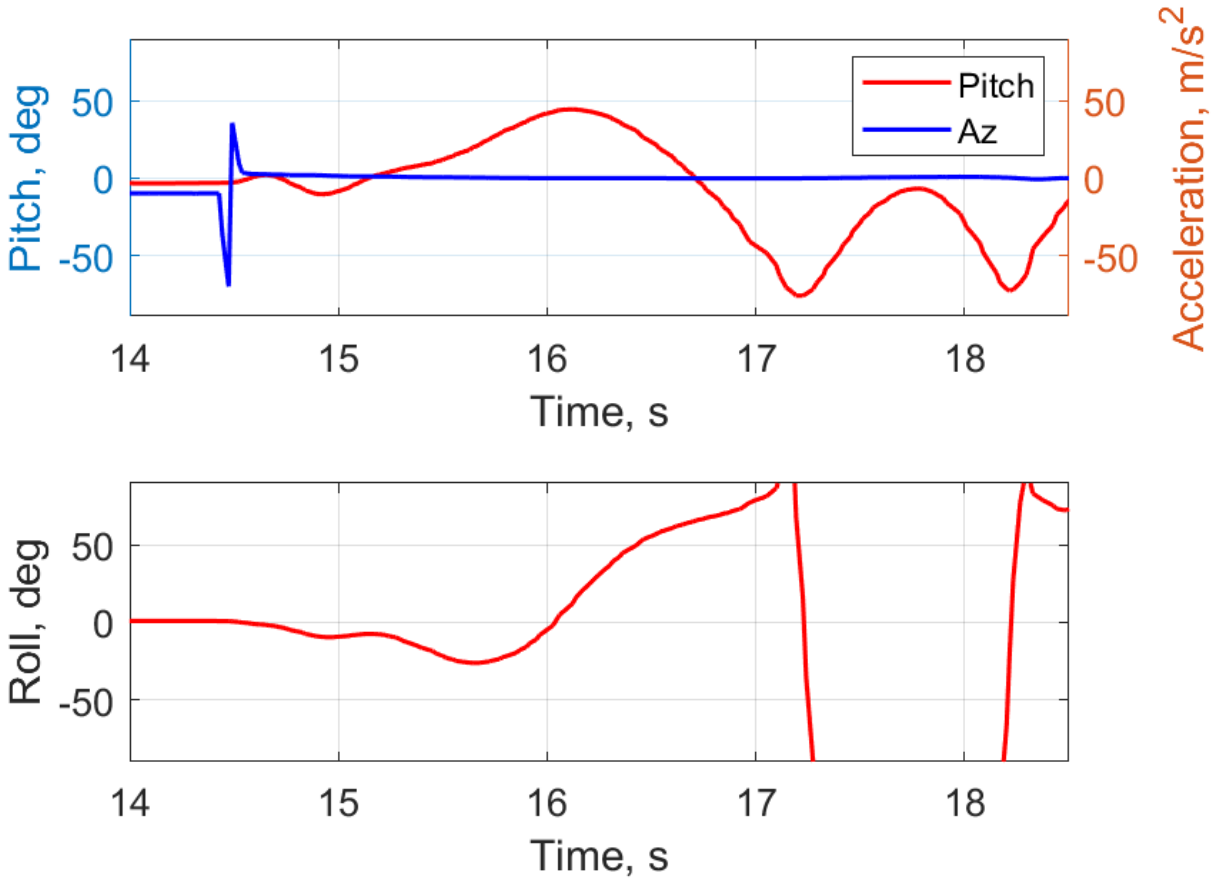

Figure 9.2: Attitude response of dummy after launch.

9.3 Vertical Vehicle Launch Testing

After all these tests mentioned above were successfully completed, the vehicle was ready for the vertical launch. This final experiment would test all of the vehicle subsystem from the thrust-vectoring mechanism to feedback controller to the rotor startup sequence. All of these systems would have to work together in concert to achieve a successful vertical launch.

9.3.1 Vertical Launch Methodology

Similar to the dummy test, the cannon was pressurized to 70 psi (482 kPa), and the cannon was positioned at a near vertical angle. After plugging in the vehicle battery, the rotors were folded, and the rotor startup sequence was checked on last time. The ground link between the ground station and the autopilot was established, and the controller gains and trim valued were checked. Before loading the vehicle into the cannon, the pilot checked all of the control inputs to ensure the appropriate response. The rotor were folded again, and the vehicle was lowered into the cannon with the fin assembly pointing down. The vehicle was launched by triggering the solenoid.

9.4 Vertical Launch Results

When the vehicle was launched, the fin was able to keep the vehicle relatively stable up to the apex of the vertical trajectory. At that point, the pilot provided a throttle command to begin the rotor startup sequence, and the sequence was captured in Fig. 9.3. As expected, the upper rotor began spinning first followed by the lower rotor, and controller began to stabilize the vehicle.

During the launch, the vehicle began tumbling shortly after rotor startup, but after a few seconds, the controller was able to stabilize the vehicle. This particular launch, that can be seen in Ref. 39, demonstrated that the vehicle could even recover from an arbitrarily large attitude angle. The pitch and roll response of the vehicle is plotted in Fig. 9.4. The plot shows that the launched occurred at the 36.5 second mark denoted by the initial spike in the blue line, and the attitude data prior to the rotor deployment are similar to the ascent phase of the dummy.

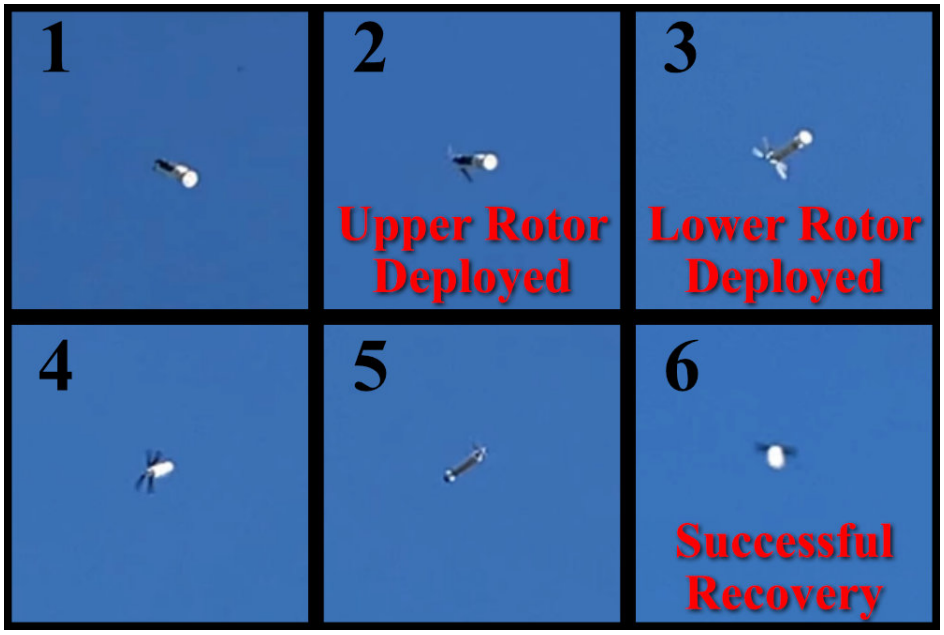

Figure 9.3: Vehicle recovery sequence after launch.

9.5 Vehicle Vertical Launch Conclusions

This chapter presented the vertical launch demonstration of a tube-launched MAV. This includes a rehearsal launch experiment with a dummy to ensure the passive stability of the system. Finally, the vehicle was launched vertically from a pneumatic cannon, and the rotor startup sequence performed as expected. Despite, the initial uncontrolled tumble during rotor spin-up, the controller was able to stabilize the vehicle and continue flying before being recovered. A successful vertical launch was considered to be a crucial milestone in achieving the final objective of a tube-launched system by demonstrating the ability to:

1. Launch the vehicle from a small tube at high accelerations.
2. Stabilize the vehicle during the projectile phase using a fin assembly that does not protrude out of the vehicle profile.
3. Passively deploy the rotors in flight using the centrifugal force.
4. Recover the vehicle from the ballistic phase and bring it to a stable hover.

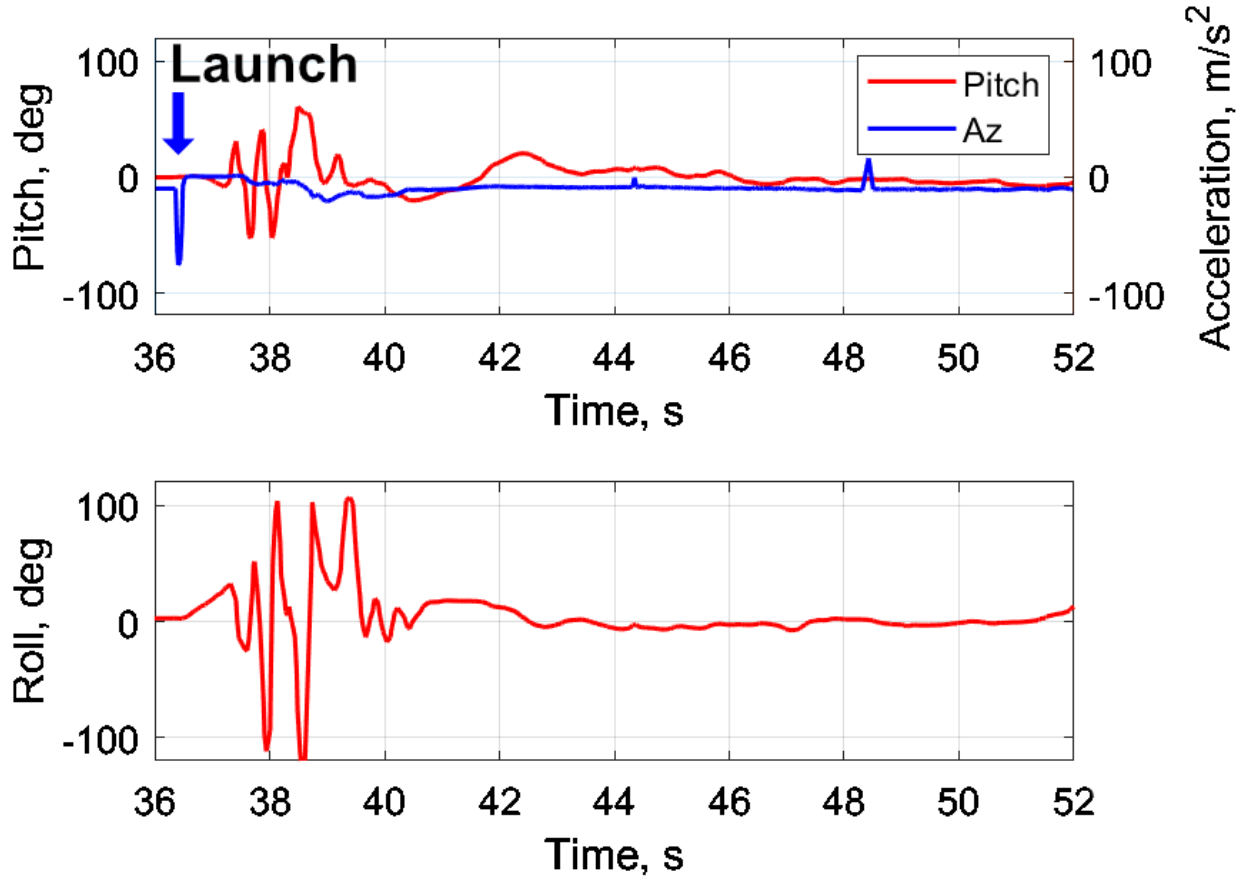

Figure 9.4: Vehicle attitude response during vertical launch and recovery. Launch occurred at 36.5 seconds.

10. CONCLUSIONS AND FUTURE WORK

This thesis described the development and flight testing of a compact, re-configurable, rotary-wing micro air vehicle concept capable of sustained hover and could potentially be launched from a 40mm grenade launcher when scaled down. This launch mechanism could be used to significantly improve range and altitude capabilities of the future MAVs. A prototype vehicle was constructed to demonstrate a vertical launch, which is an important step towards developing a ballistic launch capable vehicle. The vehicle configuration was coaxial helicopter with a thrust-vectoring mechanism for pitch and roll control in place of the usual swashplate. The thrust-vectoring design reduced the complexity of the system thereby improving reliability. The vehicle was propelled by a pair of fixed pitch counter-rotating rotors mounted to a specialized coaxial motor unit. The rotor performance was measured on a hover test stand both in the single rotor and coaxial configurations. A test vehicle was place in a wind tunnel on a single-degree-of-freedom stand to observe and tune the response of the pitch feedback controller in forward flight and axial descent. The vehicle was later tested in free flight, and the controller was tuned further. Dummy vehicle launches demonstrated the passive stability of the vehicle with a fin assembly and the viability of the rotor deployment sequence required to transition out of projectile flight. The results from all of these tests were applied to realize a successful vertical launch. This represents a major milestone on the road toward a ballistic launch and transition from the projectile phase to stable hover flight.

10.1 Conclusions

Specific conclusions from the development and testing of the Tube-launched MAV include:

1. A compact and mechanically simple thrust-vectoring mechanism used in place of swashplate for pitch and roll control was demonstrated. Pitch and roll control moments were generated by tilting the rotor plane which created moments about the CG.

2. Single and coaxial rotor experiments showed that the 3D printed rotor could withstand the aerodynamic loads and produce sufficient thrust for the vehicle.

3. A staggered rotor startup sequence prevented the upper and lower rotor from impacting each other during deployment. Rotor deployment of a coaxial configuration using only centrifugal force was demonstrated.

4. Wind tunnel, free flight, and vertical launch experiments demonstrated sufficient controller authority using a thrust vectoring mechanism in conjunction with cascaded feedback controller. The vehicle as able to track a desired attitude input in the presence of a 6 m/s forward wind speed.

5. An instability possible due to the vortex ring state was observed during axial descent testing. However, a cascaded PID controller was able to suppress the oscillation.

6. Although the controller could stabilize the vehicle without fins, wind tunnel testing demonstrated that the flight envelope could be expanded with fins. The oscillation noted in the axial descent phase could be reduced with the addition of fins on the vehicle.

7. The final vertical launch experiment demonstrated that the vehicle could even recover from arbitrarily large attitude angles after rotor startup. The controller and thrust-vectoring mechanism managed to stabilize the vehicle after it began to tumble shortly after launch.

8. The in-flight drop test and vertical launch demonstrated the ability to brake the vehicle using rotor thrust at high rates of descent without a drag device. The rotor thrust alone is enough for a controlled descent.

10.2 Future Work

After successfully demonstrating the hover capability and successful recovery of the vehicle from a vertical launch, a set of next steps are laid out below to systematically approach the final demonstration of the complete tube-launched concept.

1. Develop a process to automate the timing for the rotor deployment and recovery after launch. This could be accomplished by triggering the rotor startup sequence when the IMU, GPS, or a barometer detects the apex of the flight.

2. Launch the actual flying vehicle at an angle much lesser that 90 degrees to demonstrate transition from the projectile phase to the hover phase.

3. Once the full flight profile (launch, projectile flight, transition and hover) is successfully demonstrated, the vehicle will be redesigned to fit within the initial 40mm constraint of the grenade launcher barrel.

4. Harden the vehicle structure and electronics so that they can handle the higher acceleration loads associated with the grenade launcher.

5. Optimize the rotor design in conjunction with the electric powertrain to increase the overall endurance of the platform.

REFERENCES

[1] National Oceanic and Atmospheric Administration, “Joe cione of noaa with a coyote.” https://commons.wikimedia.org/wiki/File:Joe_cione_and_coyote_uas_in_noaa_aircraft_operation_center_credit-_noaa.jpg, "(accessed June 2020)".

[2] V. Hrishikeshavan and I. Chopra, “Refined lightweight inertial navigation system for micro air vehicle applications,” *International Journal of Micro Air Vehicles*, vol. 9, no. 2, pp. 124–135, 2017.

[3] J. McMichael and M. Francis, “Micro air vehicles - toward a new dimension in flight,” technical report, Defense Advanced Research Projects Agency, 08 1997.

[4] D. Pines and F. Bohorquez, “Challenges facing future micro-air-vehicle development,” *Journal of Aircraft*, vol. 43, no. 2, pp. 290–305, 2006.

[5] V. Kumar and N. Michael, “Opportunities and challenges with autonomous micro aerial vehicles,” *The International Journal of Robotics Research*, vol. 31, no. 11, pp. 1279–1291, 2012.

[6] V. Hauschild, “Foot marching, load carriage, and injury risk,” technical report, Army Public Health Center, 06 2016.

[7] J. M. Winslow, “Understanding of low reynolds number aerodynamics and design of micro rotary-wing air vehicles,” Master’s thesis, University of Maryland, College Park, MD, 2016.

[8] J. Winslow, M. Benedict, V. Hrishikeshavan, and I. Chopra, “Design, development, and flight testing of a high endurance micro quadrotor helicopter,” *International Journal of Micro Air Vehicles*, vol. 8, no. 3, pp. 155–169, 2016.

[9] M. Ramasamy, B. Johnson, and J. Leishman, “Understanding the aerodynamic efficiency of a hovering micro-rotor,” *Journal of The American Helicopter Society*, vol. 53, 10 2008.

[10] A. Kushleyev, D. Mellinger, C. Powers, and V. Kumar, "Towards a swarm of agile micro quadrotors," *Autonomous Robots*, vol. 35, no. 4, pp. 287–300, 2013.

[11] P. Gnemmi, S. Changey, K. Meder, E. Roussel, C. Rey, C. Steinbach, and C. Berner, "Conception and manufacturing of a projectile-drone hybrid system," *IEEE/ASME Transactions on Mechatronics*, vol. 22, no. 2, pp. 940–951, 2017.

[12] Raytheon, "Coyote uas." `https://www.raytheonmissilesanddefense.com/capabilities/products/coyote`, (accessed June 2020).

[13] AeroViroment, "Blackwing." `https://www.avinc.com/tms/blackwing`, (accessed June 2020).

[14] L. Martin, "Outrider." `https://www.lockheedmartin.com/en-gb/products/outrider.html`, (accessed September 2020).

[15] AeroViroment, "Switchblade." `https://www.avinc.com/tms/switchblade`, (accessed June 2020).

[16] UVision, "Hero-250." `https://uvisionuav.com/portfolio-view/hero-250/`, (accessed September 2020).

[17] D. Pastor, J. Izraelevitz, P. Nadan, A. Bouman, J. Burdick, and B. Kennedy, "Design of a ballistically-launched foldable multirotor," in *2019 IEEE/RSJ International Conference on Intelligent Robots and Systems (IROS)*, pp. 5212–5218, 2019.

[18] A. Bouman, P. Nadan, M. Anderson, D. Pastor, J. Izraelevitz, J. Burdick, and B. Kennedy, "Design and autonomous stabilization of a ballistically launched multirotor," *arXiv*, 11 2019.

[19] P. Gnemmi, K. Meder, and C. Rey, "Aerodynamic performance of a gun launched micro air vehicle," *International Journal of Micro Air Vehicles*, vol. 4, no. 4, pp. 251–272, 2012.

[20] P. Gnemmi, S. Changey, P. Wey, E. Roussel, C. Rey, M. Boutayeb, and R. Lozano, "Flight phases with tests of a projectile-drone hybrid system," *IEEE Transactions on Control Systems Technology*, vol. PP, pp. 1–15, 09 2017.

[21] A. Koehl, H. Rafaralahy, M. Boutayeb, and B. Martinez, "Aerodynamic modelling, estimation and control of a coaxial rotor unmanned aerial vehicle," *Journal of Intelligent & Robotic Systems*, vol. 68, pp. 53–68, 09 2012.

[22] P. Gnemmi, A. Koehl, B. Martinez, S. Changey, and S. Theodoulis, "Modeling and Control of Two GLMAV Hover-Flight Concepts," in *European Micro Aerial Vehicle Conference, EMAV 2009*, (Delft, Netherlands), pp. CD–ROM, Sept. 2009.

[23] H. Denton, M. Benedict, H. Kang, and V. Hrishikeshavan, "Development of a gun-launched rotary-wing micro air vehicle," in *Vertical Flight Society 75th Annual Forum Proceedings*, (Philadelphia, PA), 2019.

[24] H. Denton, M. Benedict, H. Kang, and V. Hrishikeshavan, "Design, development and flight testing of a gun-launched rotary-wing micro air vehicle," in *Vertical Flight Society 76th Annual Forum Proceedings*, (Virginia Beach, VA), 2020.

[25] N. Wereley and D. Pines, "Feasibility study of a smart submunition: Deployment from a conventional weapon," technical report, Army Research Laboratory, 06 2001.

[26] D. W. Kurtz and J. E. Marte, "A review of aerodynamic noise from propellers, rotors, and lift fans," technical report, NASA, 01 1970.

[27] HobbyKing.com, "Cr23m contra rotating bl system1550kv." `https://hobbyking.com/en_us/cr23m-contra-rotating-bl-system1550kv.html`, (accessed September 2019).

[28] J. Molnár, D. Drabiščák, P. Jacko, M. Guzan, and M. Maliakova, "Design of motor speed controller of electronic commutation," in *2017 International Conference on Modern Electrical and Energy Systems (MEES)*, pp. 276–279, 2017.

[29] F. Bohorquez, "Rotor hover performance and system design of an efficient coaxial rotary wing micro air vehicle," PhD dissertation, University of Maryland, College Park, MD, 2007.

[30] Prusa Research, "The original prusa i3 mk3 3d printer." `https://www.prusa3d.com/original-prusa-i3-mk3/`, (accessed August 2018).

[31] J. G. Leishman, *Principles of Helicopter Aerodynamics*. New York: Cambridge University Press, 2 ed., 2006.

[32] J. Georgy, A. Noureldin, M. Korenberg, and M. Bayoumi, "Modeling the stochastic drift of a mems-based gyroscope in gyro/odometer/gps integrated navigation," *IEEE Transactions on Intelligent Transportation Systems*, vol. 11, no. 4, pp. 856–872, 2010.

[33] Y. K. Thong, M. S. Woolfson, J. A. Crowe, B. R. Hayes-Gill, and R. E. Challis, "Dependence of inertial measurements of distance on accelerometer noise," *Measurement Science and Technology*, vol. 13, pp. 1163–1172, jul 2002.

[34] D. Schmidt, *Modern Flight Dynamics*. McGraw-Hill Education, 2011.

[35] H. Denton and M. Benedict, "Tube-launched, coaxial helicopter mav: Rotor startup sequence." `https://youtu.be/pGweDj1IoJk`, 2020.

[36] H. Denton and M. Benedict, "Tube-launched, coaxial helicopter mav: Vertical dummy launch 75 psi." `https://youtu.be/04gfYwxBXoQ`, 2020.

[37] H. Denton and M. Benedict, "Tube-launched, coaxial helicopter mav: Wind tunnel disturbance testing." `https://youtu.be/IRb5iy6iRQ0`, 2020.

[38] H. Denton and M. Benedict, "Tube-launched, coaxial helicopter mav: In-flight drop test." `https://youtu.be/GV2YsQYY-Dc`, 2020.

[39] H. Denton and M. Benedict, "Tube-launched, coaxial helicopter mav: Vertical launch." `https://youtu.be/PXTo6DkNsr8`, 2020.